enhanced the formation of lamellipodia with membrane ruffling is also consistent with the involvement of Capn6 in microtubule stability. Previous reports have demonstrated that changes in microtubule stability affect cell motility through microtubule-actin interactions (34). For example, Hubbert et al. have shown that deacetylation of α-tubulin by HDAC6 promotes chemotactic cell migration (17). Waterman-Storer et al. have provided a model in which the growth phase of microtubule dynamic instability drives actin polymerization and lamellipodial protrusion via Rac1 activation (39). Taken together with these findings, the present results suggest that Capn6 may be involved in the control of microtubule dynamic instability and actin organization.

How can Capn6 induce microtubule stabilization? It is unlikely that Capn6 has a concealed protease activity by which it may modulate microtubule dynamics, because calpain inhibitors did not inhibit Capn6-induced microtubule bundling. Rather, Capn6 may exert its effect by antagonizing other calpains as a nonproteolytic family member. Indeed, the stability of microtubules is enhanced by MAPs (6, 18), which are in vitro calpain substrates. Rho GTPase, another possible calpain substrate (20), and its effector, mDia, also have microtubule-stabilizing properties (3, 31). It would be worthwhile to test whether Capn6 may protect these microtubule-stabilizing factors from proteolysis in the restricted cytoskeletal regions. It is also possible that Capn6 may stabilize microtubules through an as-yet-unknown function independent of protease activity. For example, the pattern of microtubule bundling may suggest possible interactions between Capn6 and other signaling pathways. Capn6-transfected cells exhibited stable microtubule bundling predominantly in the perinuclear region. Remarkably, a similar pattern of microtubule bundling is induced by certain members of sterile 20 (STE20)-like kinases. *Xenopus* p21-activated kinase 5 (X-PAK5), a Cdc42/Rac effector, colocalizes to microtubules and promotes the formation of stable microtubule bundles around the nucleus (1). Prostate-derived STE20-like kinase, a member of the germinal-center kinase-like kinase subfamily, also produces perinuclear microtubule bundles (27). These kinases are also involved in the regulation of actin organization, suggesting that they may play roles in the cross talk between microtubules and the actin cytoskeleton. Although the role of Capn6 in the regulation of actin organization has not yet been determined, the enhanced lamellipodium formation induced by Capn6 silencing may suggest the possible involvement of Capn6 in this cytoskeletal cross talk.

Is Capn6 involved in embryogenesis through its microtubule-stabilizing effect? The answer to this question remains unknown, although Capn6 was identified as a molecule in the genetic hierarchy controlling pharyngeal-arch development. In this respect, it is noteworthy that cytoskeletal remodeling, including microtubules, is involved in various processes during animal development. For example, Rho family GTPase-regulating proteins required for cytokinesis have also emerged as modulators of cytoskeletal reorganization in transitions between the epithelium and mesenchyme in either direction (23). It is possible that Capn6, expressed in the pharyngeal-arch epithelium and mesenchyme, participates in developmental processes involving cytoskeletal reorganization in cooperation with these proteins. Further investigations using a gene-targeting approach are expected to clarify the link between the molecular functions of Capn6 and developmental processes.

ACKNOWLEDGMENTS

We thank Hideyuki Saya (Kumamoto University), Yoshimitsu Kanai, and Yasuko Noda (The University of Tokyo) for technical advice and helpful discussion. K.T. is a Research Fellow of the Japan Society for the Promotion of Science (DC1).

This work was supported by grants from the Japan Society for the Promotion of Science Research for the Future Program; grants-in-aid for scientific research from the Ministry of Education, Culture, Sports, Science and Technology, Japan; and a Research Grant from the Uehara Memorial Foundation.

REFERENCES

1. **Cau, J., S. Faure, M. Comps, C. Delsert, and N. Morin.** 2001. A novel p21-activated kinase binds the actin and microtubule networks and induces microtubule organization. J. Cell Biol. **155**:1029–1042.
2. **Clouthier, D. E., K. Hosoda, J. A. Richardson, S. C. Williams, H. Yanagisawa, T. Kuwaki, M. Kumada, R. E. Hammer, and M. Yanagisawa.** 1998. Cranial and cardiac neural crest defects in endothelin-A receptor-deficient mice. Development **125**:813–824.
3. **Cook, T. A., T. Nagasaki, and G. G. Gundersen.** 1998. Rho guanosine triphosphatase mediates the selective stabilization of microtubules induced by lysophosphatidic acid. J. Cell Biol. **141**:175–185.
4. **Dear, N., K. Matena, M. Vingron, and T. Boehm.** 1997. A new subfamily of vertebrate calpains lacking a calmodulin-like domain: implications for calpain regulation and evolution. Genomics **45**:175–184.
5. **Dear, T. N., and T. Boehm.** 1999. Diverse mRNA expression patterns of the mouse calpain genes Capn5, Capn6 and Capn11 during development. Mech. Dev. **89**:201–209.
6. **Drewes, G., A. Ebneth, and E.-M. Mandelkow.** 1998. MAPs, MARKs and microtubule dynamics. Trends Biochem. Sci. **23**:307–311.
7. **Fukuhara, S., Y. Kurihara, Y. Arima, N. Yamada, and H. Kurihara.** 2004. Temporal requirement of signaling cascade involving endothelin-1/endothelin A receptor in branchial arch development. Mech. Dev. **121**:1223–1233.
8. **Gil-Parrado, S., O. Popp, T. A. Knoch, S. Zahler, F. Bestvater, M. Felgentrager, A. Holloschi, A. Fernandez-Montalvan, E. A. Auerswald, H. Fritz, P. Fuentes-Prior, W. Machleidt, and E. Spiess.** 2003. Subcellular localization and in vivo subunit interactions of ubiquitous μ-calpain. J. Biol. Chem. **278**:16336–16346.
9. **Glading, A., D. A. Lauffenburger, and A. Wells.** 2002. Cutting to the chase: calpain proteases in cell motility. Trends Cell Biol. **12**:46–54.
10. **Glotzer, M.** 2005. The molecular requirements for cytokinesis. Science **307**: 1735–1739.
11. **Goll, D. E., V. F. Thompson, H. Li, W. Wei, and J. Cong.** 2003. The calpain system. Physiol. Rev. **83**:731–801.
12. **Higuchi, M., N. Iwata, and T. C. Saido.** 2005. Understanding molecular mechanisms of proteolysis in Alzheimer's disease: progress toward therapeutic interventions. Biochim. Biophys. Acta **1751**:60–67.
13. **Hosfield, C. M., J. S. Elce, P. L. Davies, and Z. Jia.** 1999. Crystal structure of calpain reveals the structural basis for Ca^{2+}-dependent protease activity and a novel mode of enzyme activation. EMBO J. **18**:6880–6889.
14. **Hosfield, C. M., T. Moldoveanu, P. L. Davies, J. S. Elce, and Z. Jia.** 2001. Calpain mutants with increased Ca^{2+} sensitivity and implications for the role of the C_2-like domain. J. Biol. Chem. **276**:7404–7407.
15. **Hosfield, C. M, J. S. Elce, and Z. Jia.** 2004. Activation of calpain by Ca^{2+}: roles of the large subunit N-terminal and domain III-IV linker peptides. J. Mol. Biol. **343**:1049–1053.
16. **Huang, Y., and K. K. Wang.** 2001. The calpain family and human disease. Trends Mol. Med. **7**:355–362.
17. **Hubbert, C., A. Guardiola, R. Shao, Y. Kawaguchi, A. Ito, A. Nixon, M. Yoshida, X. F. Wang, and T. P. Yao.** 2002. HDAC6 is a microtubule-associated deacetylase. Nature **417**:455–458.
18. **Kaech, S., B. Ludin, and A. Matus.** 1996. Cytoskeletal plasticity in cells expressing neuronal microtubule-associated proteins. Neuron **17**:1189–1199.
19. **Kimmel, C. B., B. Ullmann, M. Walker, C. T. Miller, and J. G. Crump.** 2003. Endothelin 1-mediated regulation of branchial bone development in zebrafish. Development **130**:1339–1351.
20. **Kulkarni, S., D. E. Goll, and J. E. Fox.** 2002. Calpain cleaves RhoA generating a dominant-negative form that inhibits integrin-induced actin filament assembly and cell spreading. J. Biol. Chem. **277**:24435–24441.
21. **Kurihara, Y., H. Kurihara, H. Suzuki, T. Kodama, K. Maemura, R. Nagai, H. Oda, T. Kuwaki, W.-H. Cao, N. Kamada, K. Jishage, Y. Ouchi, S. Azuma, Y. Toyoda, T. Ishikawa, M. Kumada, and Y. Yazaki.** 1994. Elevated blood pressure and craniofacial abnormalities in mice deficient in endothelin-1. Nature **368**:703–710.
22. **Kurihara, Y., H. Kurihara, H. Oda, K. Maemura, R. Nagai, T. Ishikawa, and**

Y. Yazaki. 1995. Aortic arch malformations and ventricular septal defect in mice deficient in endothelin-1. J. Clin. Investig. **96:**293–300.
23. **Labouesse, M.** 2004. Epithelium-mesenchyme: a balancing act of RhoGAP and RhoGEF. Curr. Biol. **14:**R508–R510.
24. **Lane, R. D., D. M. Allan, and R. L. Mellgren.** 1992. A comparison of the intracellular distribution of μ-calpain, m-calpain, and calpastatin in proliferating human A431 cells. Exp. Cell Res. **203:**5–16.
25. **Masaki, T.** 2004. Historical review: endothelin. Trends Pharmacol. Sci. **25:** 219–224.
26. **Matena, K., T. Boehm, and N. Dear.** 1998. Genomic organization of mouse Capn5 and Capn6 genes confirms that they are a distinct calpain subfamily. Genomics **48:**117–120.
27. **Mitsopoulos, C., C. Zihni, R. Garg, A. J. Ridley, and J. D. H. Morris.** 2003. The prostate-derived sterile 20-like kinase (PSK) regulates microtubule organization and stability. J. Biol. Chem. **278:**18085–18091.
28. **Nakaseko, Y., K. Nabeshima, K. Kinoshita, and M. Yanagida.** 1996. Dissection of fission yeast microtubule associating protein $p93^{Dis1}$: regions implicated in regulated localization and microtubule interaction. Genes Cells **1:**633–644.
29. **Ozeki, H., Y. Kurihara, K. Tonami, S. Watatani, and H. Kurihara.** 2004. Endothelin-1 regulates the dorsoventral branchial arch patterning in mice. Mech. Dev. **121:**387–395.
30. **Pal, G. P., T. De Veyra, J. S. Elce, and Z. Jia.** 2003. Crystal structure of a micro-like calpain reveals a partially activated conformation with low Ca^{2+} requirement. Structure **11:**1521–1526.
31. **Palazzo, A. F., T. A. Cook, A. S. Alberts, and G. G. Gundersen.** 2001. mDia mediates Rho-regulated formation and orientation of stable microtubules. Nat. Cell Biol. **3:**723–729.
32. **Piperno, G., M. LeDizet, and X. J. Chang.** 1987. Microtubules containing acetylated alpha-tubulin in mammalian cells in culture. J. Cell Biol. **104:**289–302.
33. **Rizo, J., and T. C. Südhof.** 1998. C_2-domains, structure and function of a universal Ca^{2+}-binding domain. J. Biol. Chem. **273:**15879–15882.
34. **Rodriguez, O. C., A. W. Schaefer, C. A. Mandato, P. Forscher, W. M. Bement, and C. M. Waterman-Storer.** 2003. Conserved microtubule-actin interactions in cell movement and morphogenesis. Nat. Cell Biol. **5:**599–609.
35. **Sorimachi, H., S. Ishiura, and K. Suzuki.** 1997. Structure and physiological function of calpains. Biochem. J. **328:**721–732.
36. **Sorimachi, H., and K. Suzuki.** 2001. The structure of calpain. J. Biochem. (Tokyo) **129:**653–664.
37. **Strobl, S., C. Fernandez-Catalan, M. Braun, R. Huber, H. Masumoto, K. Nakagawa, A. Irie, H. Sorimachi, G. Bourenkow, H. Bartunik, K. Suzuki, and W. Bode.** 2000. The crystal structure of calcium-free human m-calpain suggests an electrostatic switch mechanism for activation by calcium. Proc. Natl. Acad. Sci. USA **97:**588–592.
38. **Suzuki, K., and H. Sorimachi.** 1998. A novel aspect of calpain activation. FEBS Lett. **433:**1–4.
39. **Waterman-Storer, C. M., R. A. Worthylake, B. P. Liu, K. Burridge, and E. D. Salmon.** 1999. Microtubule growth activates Rac1 to promote lamellipodial protrusion in fibroblasts. Nat. Cell Biol. **1:**45–50.
40. **Webster, D. R., and J. M. Bratcher.** 2006. Developmental regulation of cardiac MAP4 protein expression. Cell Motil. Cytoskeleton **63:**512–522.
41. **Wilkinson, D.** 1992. *In situ* hybridisation: a practical approach. IRL Press, Oxford, United Kingdom.
42. **Yanagisawa, M., H. Kurihara, S. Kimura, Y. Tomobe, M. Kobayashi, Y. Mitsui, Y. Yazaki, K. Goto, and T. Masaki.** 1988. A novel potent vasoconstrictor peptide produced by vascular endothelial cells. Nature **332:**411–415.

Current Topics

Metabolism and Functions of Phosphoinositides

Role of Phosphatidylinositol 3-Kinase Activation on Insulin Action and Its Alteration in Diabetic Conditions

Tomoichiro ASANO,*[,a] Midori FUJISHIRO,[b] Akifumi KUSHIYAMA,[b] Yusuke NAKATSU,[a] Masayasu YONEDA,[a] Hideaki KAMATA,[a] and Hideyuki SAKODA[b]

[a] *Division of Molecular Medical Science, Graduate School of Biomedical Sciences, Hiroshima University; 1–2–3 Kasumi, Minami-ku, Hiroshima, Hiroshima 734–8551, Japan: and* [b] *Department of Internal Medicine, Graduate School of Medicine, University of Tokyo; 7–3–1 Hongo, Bunkyo-ku, Tokyo 113–8655, Japan.*

Received July 9, 2007

Inositol phospholipids phosphorylated on D3-position of their inositol rings (3-phosphoinositides) are known to play important roles in various cellular events. Activation of PI (phosphatidylinositol) 3-kinase is essential for aspects of insulin-induced glucose metabolism, including translocation of GLUT4 to the cell surface and glycogen synthesis. The enzyme exists as a heterodimer containing a regulatory subunit and one of two widely-distributed isoforms of the p110 catalytic subunit: p110α or p110β. Activation of PI 3-kinase and its downstream AKT has been demonstrated to be essential for almost all of the insulin-induced glucose and lipid metabolism such as glucose uptake, glycogen synthesis, suppression of glucose output and triglyceride synthesis as well as insulin-induced mitogenesis. Accumulated PI(3,4,5)P_3 activates several serine/threonine kinases containing a PH (pleckstrin homology) domain, including Akt, atypical PKCs, p70S6 kinase and GSK.

In the obesity-induced insulin resistant condition, JNK and p70S6K are activated and phosphorylate IRS-proteins, which diminishes the insulin-induced tyrosine phosphorylation of IRS-proteins and thereby impairs the PI 3-kinase/AKT activations. Thus, the drugs which restore the impaired insulin-induced PI 3-kinase/AKT activation, for example, by suppressing JNK or p70S6K, PTEN or SHIP2, could be novel agents to treat diabetes mellitus.

Key words insulin; PI 3-kinase; diabetes mellitus; insulin resistance

1. INTRODUCTION

The insulin receptor is a transmembrane glycoprotein that mediates the first step in insulin action. When insulin binds to the extracellular domain of the receptor, the intrinsic tyrosine kinase activity of the intracellular domain of the receptor is activated. Then, the activated insulin receptor tyrosine kinase phosphorylates several tyrosine residues of the insulin receptor itself, as well as several intracellular substrates. This review describes how these intracellular substrates transmit the signals necessary to induce various metabolic actions of insulin.

Insulin resistance plays a major role in the occurrence and development of Type 2 diabetes mellitus, which accounts for over 85% of diabetes worldwide. As insulin resistance develops, pancreatic β-cells compensate by secreting more insulin until their capacity to produce adequate amounts of the hormone is exhausted, and the elevation of blood glucose becomes manifest.

Although very probably there are many genetic factors affecting insulin sensitivity in humans, it is well-known that insulin sensitivity is also affected by environmental factors closely linked to modern civilization, by affluence and by increased life expectancy. All of the aforementioned factors contribute to insulin resistance, and that they reflect a variety of molecular mechanisms. There have been a number of recent studies investigating the intracellular signaling pathway leading from the binding of insulin to its receptor to activation of glucose and lipid metabolisms.

2. INSULIN-INDUCED PI 3-KINASE ACTIVATION IS MEDIATED BY IRS-PROTEINS

The principal insulin receptor substrates, called IRS-proteins, are phosphorylated on multiple tyrosine residues by the activated insulin receptor. The IRS-protein family consists of at least 4 isoforms, termed IRS-1, 2, 3 and 4.[1] These IRS-proteins possess a PH domain and a PTB domain at their N-termini, and associate with the insulin receptor *via* these domains. Phosphorylated IRS-proteins recruit various signaling proteins into a multicomponent complex through the interaction between their phosphotyrosine-containing motifs and the SH2 domain of downstream signaling molecules. These SH2-containing proteins include the regulatory subunit of the PI 3-kinase, Grb2, SHP-2, fyn, and others.[1] In addition, it was shown that 14-3-3 protein recognizes and binds to the phosphorylated serine containing motif of IRS-proteins.[2] This association with 14-3-3 protein inhibits the association of IRS-1 with the insulin receptor and resultant tyrosine phosphorylation. Thus, this mechanism may be important for regulating the functions of IRS-proteins, particularly transfer of the signal from the insulin receptor to downstream factors. Although other SH2 proteins also bind to IRS-1/2, PI 3-kinase is considered to be particularly important for the insulin-induced glucose uptake into muscle and adipose tissue, which is dependent on the translocation of a glucose transporter to the plasma membrane. Indeed, the overexpression of constitutively-active, membrane-targeted or GLUT2-tagged p110α increased translocation of GLUT4 glucose

* To whom correspondence should be addressed. e-mail: tasano@hiroshima-u.ac.jp

transporter to the cell surface and increased basal glucose transport, irrespective of the presence of insulin.[3—5] Treatment with specific inhibitors of PI 3-kinase or overexpression of the dominant negative form of the PI 3-kinase regulatory subunit inhibited insulin-induced glucose uptake, glycogen synthesis and DNA synthesis. In addition, PI 3-kinase activation also reportedly plays an important role in insulin-induced glycogen synthesis and suppression of phosphoenolpyruvate carboxykinase (PEPCK) expression in hepatocytes.[6—8] Thus, PI 3-kinase activation is considered to play a critical role in insulin-induced glucose metabolism in muscle, fat, and liver.

Although many growth factors and hormones similarly activate PI 3-kinase, it should be noted that insulin is the only hormone which effectively induces glucose metabolism. This difference can be explained as followings; insulin-induced activated PI 3-kinase is translocated to the specific intracellular place with the associated IRS-1 or IRS-2, while many growth factor receptors such as PDGF (platelet derived growth factor) receptor induces the activation of PI 3-kinase at the plasma membrane with a direct association of PI 3- kinase with the receptor on the plasma membrane. Thus, such different location in the activated PI 3-kinase is considered to induce the different response for the glucose metabolism. Furthermore, interestingly, IRS-1 and IRS-2 reportedly exhibit the different subcellular distribution although not shown very clearly,[9] and analysis using IRS-1 and IRS-2 KO mice demonstrated that IRS-1 is important for insulin-induced metabolism in the muscle and adipose tissue, while IRS-2 in the liver and pancreatic β cells.[10]

3. STRUCTURE OF PI 3-KINASES

PI 3-kinase exists as a dimer composed of a 110-kDa catalytic subunit associated with a regulatory subunit (Fig. 1). Activated receptors with tyrosine kinase activity often interact with regulatory subunit SH2 domains *via* phosphorylated YXXM motifs,[11] in turn activating or recruiting PI 3-kinase. The regulatory subunit contains two proline-rich motifs (PRMs), two SH2 domains and a domain (IS) situated between the SH2 domains, which is responsible for binding to p110.[12] To date, five isoforms of the regulatory subunit have been identified: two 85-kDa proteins (p85α, p85β),[12,13] two 55-kDa proteins (p55α, p55γ)[14—16] and one 50-kDa protein (p50α).[17] Interestingly, transcription of the p85β gene yields three isoforms of the regulatory subunit. The p85β and p55γ genes, by contrast, express single 85-kDa and 55-kDa protein products, respectively. Although lacking the Src-homology 3 (SH3) and BCR homology (BH) domains, a similar short form of the regulatory subunit was found in drosophila (droPIK57).[18] Such conserved expression among distant species is likely indicative of the importance of the short forms of the regulatory subunits. Structural differences in the N-terminal regions of the different group members contribute to defining their binding specificity, their subcellular distributions and their capacity to activate the 110-kDa catalytic subunit.

Two widely distributed isoforms of the catalytic subunit have been identified as p110α and p110β. On the basis of *in vitro* assays of the lipid kinase activities of p110α and p110β expressed in Sf-9 cells, basal p110α activity is substantially lower than that of p110α. However, p110β appears to be highly insulin-sensitive, while p110α was unaffected by insulin, despite the fact that both isoforms bind to the p85α subunit and to IRS-1 with similar efficiency.[19]

PI 3-kinase catalyzes the formation of PI-3-P, PI-3,4-P_2 and PI-3,4,5-P_3 from PI, PI-4-P and PI-4,5-P_2, respectively. Signaling molecules binding to PI-3,4-P_2 and PI-3,4,5-P_3 include serine/threonine kinases (PKB, PKC, PDK-1)[20—22]; guanine nucleotide exchange factors for small GTP-binding proteins (Grp1, Cytohesin1, ARNO, SOS, Tiam-1)[23—26]; protein tyrosine kinases (Src, Btk)[27,28]; and Clathrin adaptors (AP2, AP3).[29,30] Among them, Akt (also known as PKB), a serine/threonine kinase, translocates to the membrane frac-

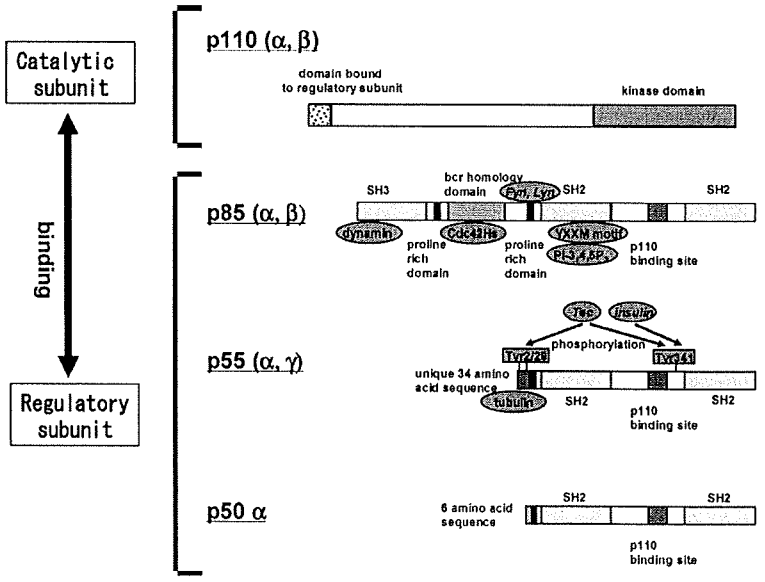

Fig. 1. Structure of the p85/p110 Type PI-Kinase
Schematic diagram showing the three classes of PI 3-kinase regulatory subunit (p85, p55 and p50) and the catalytic subunit (p110). Ellipses denote ligands binding to their respective binding sites on the subunits, while rectangles denote potential tyrosine phosphorylation sites.

tion *via* binding of the PH domain with the PI-3,4,5-P_3 produced by PI 3-kinase, and phosphorylations of Thr306 and Ser473 of Akt by PDK1[31] and Rictor/mTOR complex[32] take place thereby activating Akt kinase. This step was found to mediate various insulin- and growth factor-induced cellular responses, such as the stimulation of GLUT4 translocation to the plasma membrane, the inhibition of glycogen synthase kinase-3 (GSK-3), induction of triglyceride synthesis *via* increasing the expression of SREBP1C and the promotion of cell survival by inhibiting apoptosis.[33] Indeed, these cellular activities have been shown to be induced by overexpression of the constitutively active or the membrane targeted mutant of Akt, while Akt2-deficient mice show impaired glucose tolerance due to decreased insulin-induced glucose uptake in skeletal muscle and increased hepatic glucose production.[34] Thus, PI 3-kinase/Akt pathway is critically important for insulin-induced glucose and lipid metabolisms.

4. ALTERED INOSITOL PHOSPHOLIPID METABOLISM IN THE INSULIN RESISTANT CONDITIONS

Insulin resistance plays a major role in the occurrence and development of Type 2 diabetes mellitus, which accounts for over 85% of diabetes worldwide. As insulin resistance develops, pancreatic β-cells compensate by secreting more insulin until their capacity to produce adequate amounts of the hormone is eventually exhausted, and blood glucose elevation manifests.

It is well-known that insulin sensitivity is also affected by environmental factors closely linked to modern civilization, as well as mostly unidentified genetic factors. Once diabetes mellitus worsens, prolonged hyperglycemia is itself a factor diminishing insulin sensitivity. Consequently, any individual case of Type 2 diabetes mellitus will usually involve two or more factors reducing the patient's insulin sensitivity. For example, excess caloric intake, high-fat diet, insufficient exercise, aging and so on all contribute to the insulin resistance observed during the early, impaired glucose tolerance (IGT) stage of Type 2 diabetes mellitus; later in the disease process, when hyperglycemia is chronic, the contribution made by elevated blood glucose may be significant.

In a later portion of this review, we describe how insulin signaling is affected by factors such as obesity with overeating, high-fat diet, hyperglycemia, and salt-related hypertension, citing results obtained using rodent models.

Impared PI 3-Kinase Activation in Zucker Fatty Obese Rats As a first step, we analyzed the impaired insulin signaling in Zucker fatty rats, which are considered to be an excellent model of early-stage Type 2 diabetes mellitus induced by overeating and overweight. Zucker rats exhibit marked hyperinsulinemia and obesity due to a leptin receptor mutation, but they have relatively mild hyperglycemia. This constellation of symptoms is very similar to that observed in the early phase of human Type 2 diabetes mellitus. The insulin resistance in Zucker fatty rats involves both impaired glucose transport in muscle and impaired suppression of glucose production in the liver.

Some studies have suggested that insulin receptor tyrosine kinase activity is impaired in the Zucker fatty rat.[35] Our results, however, suggest that the degree of impairment at this step is relatively mild, which is in agreement with the results obtained with skeletal muscles from obese non-diabetic human subjects. A more significant factor contributing to insulin resistance in Zucker fatty rats is likely to be diminished expressions of IRS-1 and IRS-2.[36] Expressions of both IRS-1 and IRS-2 mRNA and protein were found to be downregulated in both liver and muscle of Zucker fatty rats. Moreover, it appears that mRNA transcription is more severely affected than protein synthesis. Consistent with decreased synthesis, insulin-induced increases in tyrosine phosphorylation of IRS-1 and IRS-2 were reduced in both liver and muscle of Zucker fatty rats. By normalizing the tyrosine phosphorylation of IRS-1/2 per unit protein, the decline in tyrosine phosphorylation was confirmed to be due mainly to the decline in the levels of these two proteins; although with the exception of IRS-2 in muscle, impaired insulin receptor-mediated phosphorylation also played a minor role.

Tyrosine phosphorylated IRS-1/2 binds to the regulatory subunit (*e.g.*, p85α) of PI 3-kinase, thereby activating the enzyme. The insulin-induced increases in the amount of IRS-1/2-bound p85α and the corresponding increases in PI 3-kinase activity were all decreased in the livers and muscles of fatty rats.[36] Of particular importance to us was the finding that decreases in hepatic PI 3-kinase activity were more marked than the decreases in tyrosine phosphorylation or in the binding of IRS-1/2 to p85α.

The association of IRS-1/2 with PI 3-kinase occurs *via* phosphorylated YMXM or YXXM motifs on IRS-1/2 and the SH2 domains on the regulatory subunit of PI 3-kinase (Backer *et al.* 1992). For full activation of PI 3-kinase, it is necessary for both SH2 domains to be bound; binding of only one SH2 domain to a phosphorylated motif induces only partial activation. Thus, IRS-1/2 must be phosphorylated on two or more tyrosine residues in the Y(M/X)XM motifs to fully activate the associated PI 3-kinase, even though IRS-1/2 containing only a single phosphorylated Y(M/X)XM motif can bind to the enzyme. In addition, tyrosine phosphorylation of sites other than the Y(M/X)XM motifs would not contribute to the activation of PI 3-kinase, though they may be recognized by our anti-phosphotyrosine antibody. The discrepancy between the levels of IRS-1/2 tyrosine phosphorylation and the associated PI 3-kinase activities, therefore, may be explained by a selective decrease in phosphorylation of the tyrosine residues in Y(M/X)XM motifs. However, the intramolecular mechanisms regulating ty-

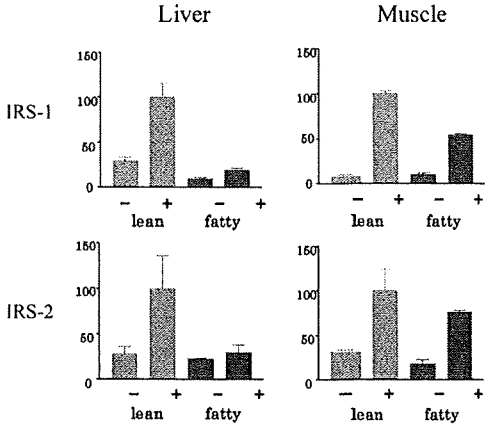

Fig. 2. Impaired p85/p110 Type PI-Kinase Activation in Zucker Fatty Rats

rosine phosphorylation sites on IRS-1/2 await clarification.

In contrast to the liver, the muscles of Zucker fatty rats showed no apparent shift in the relation between binding of IRS-1/2 to the p85α regulatory subunit and PI 3-kinase activity.

High-fat Diet Induces Tissue-Specific Alteration in Insulin Signaling Numerous studies have now confirmed that insulin action is impaired in liver, muscle and adipose tissues of rats maintained on a high-fat diet. For example, basal hepatic glucose production is increased in such rats, and insulin-induced suppression of this glucose production is impaired. With a high-fat diet, glycogen synthesis decreases in both muscle and liver, and insulin-induced glucose uptake and GLUT4 translocation to the plasma membrane are reduced in both muscle and adipose tissues. It is clear then that excessive dietary fat consumption can lead to insulin resistance in all three tissues.

The levels of IRS-1/2 protein in hepatic and muscle tissues of rats on a high-fat diet were found to be similar to those of control rats. In contrast, levels of IRS-1/2 in the epididymal fat were decreased to 55% and 65% of those in control rats.[37] Impaired insulin-stimulated tyrosine phosphorylation of IRS-1/2 has been observed in several diabetic animal models, and there was a tendency for tyrosine phosphorylation of IRS-1/2 to be decreased in the livers of rats on high-fat diets, but the difference was not statistically significant. Insulin-evoked tyrosine phosphorylation of IRS-1/2 in muscle was lower in fat-fed rats than in controls, however, and, the suppressive effect of high fat was even more pronounced in the epididymal fat. However, surprisingly, both basal and insulin-stimulated levels of IRS-1/2-bound p85α were increased in the livers of rats on high-fat diets, although phosphorylation of IRS-1/2 was unchanged. In muscle, by contrast, insulin-stimulated levels of IRS-1/2-bound p85α in rats on high-fat diets were significantly decreased to 78% and 68% of the control levels, while in the epididymal fat, the levels were down to 74% and 53% of the control levels.

The insulin-induced elevation of IRS-1/2-bound p85α seen in the livers of rats on a high-fat diet resulted in a 2-fold increase in PI 3-kinase activity, whereas the declines in IRS-1/2-bound p85α in muscle and epididymal fat resulted in concomitant, significant declines PI 3-kinase activity.

Levels of IRS-1/2 protein were unaltered in the muscles of rats fed a high-fat diet, although their phosphorylation was impaired. It is likely, therefore, that the reduced p85α binding and PI 3-kinase activity seen in the muscle tissues of rats fed a high-fat diet resulted from decreased tyrosine phosphorylation of IRS-1/2. In the case of epididymal fat, IRS-1/2 expression was reduced by 30—40% as compared to the control, which in turn led to reduced levels of tyrosine phosphorylation, reduced binding to p85α, and reduced PI 3-kinase activity. In contrast to muscle, therefore, insulin signaling is impaired mainly at the level of IRS-1/2 expression in the adipose tissues of fat-fed rats.

Hepatic expression of IRS-1/2 was not significantly altered in fat-fed rats, nor was expression of PI 3-kinase; tyrosine phosphorylation of IRS-1/2 was altered only slightly; and increased PI 3-kinase resulted from significantly augmented binding of IRS-1/2 to p85α. The fact that PI 3-kinase activation was significantly enhanced in the livers of rats fed a high-fat diet clearly indicates that such a diet causes hepatic

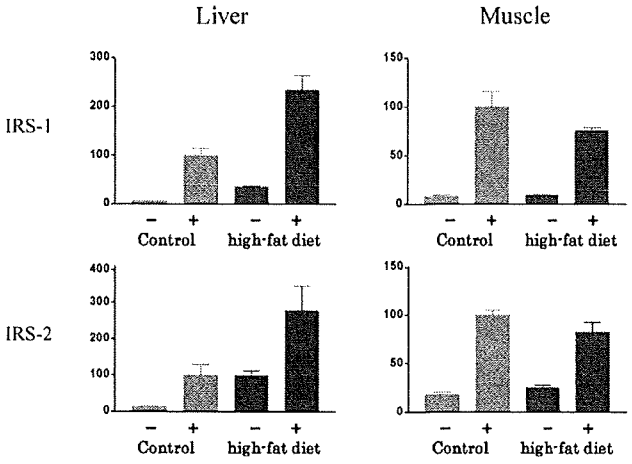

Fig. 3. PI 3-Kinase Activity in Liver and Muscle of SD Rats Maintained on High-Fat Diets

insulin resistance by a mechanism other than those underlying decreased insulin sensitivity in muscle and adipose tissues.

IRS-1/2 each contain approximately 20 putative tyrosine phosphorylation sites, only four of which are in the Y(M/X)XM motif responsible for the interaction with PI 3-kinase regulatory subunits. IRS-1/2 also contains more than 30 potential serine/threonine phosphorylation sites for casein kinase II, protein kinase C, MAP kinase and cdc2, as well as phosphorylation sites for cAMP- and cGMP-dependent protein kinases. It seems reasonable, therefore, to suggest that in rats on a high-fat diet, a change in the phosphorylation state at one or more of those other sites might upregulate the phosphorylation of specific hepatic tyrosine residues, thereby augmenting p85α binding to IRS-1/2, while phosphorylation of other tyrosine residues, or at least those efficiently recognized by the anti-phosphotyrosine antibody used in our assay, are unaffected. Alternatively, the possibility that IRS-1/2 binding to p85α is increased by an as yet unknown modification of the p85α protein—*e.g. via* serine/threonine phosphorylation(s)—cannot be excluded.

It was especially interesting to us that insulin-stimulated PI 3-kinase activity was severely impaired in the livers of other obese diabetic rodent models, such as ob/ob mice[38] and Zucker fatty rats,[36] while being enhanced in the livers of rats fed a high fat diet. The effects of a high-fat diet on insulin-stimulated PI 3-kinase activation were thus clearly opposite those of obesity induced by general overeating (*i.e.* obesity due to leptin system dysfunction), suggesting that in fat-fed rats impaired insulin action may originate downstream from PI 3-kinase activation.

Hyperglycemia-Induced Alteration in Insulin Signaling Hyperglycemia is believed to contribute to the development of peripheral insulin resistance associated with both type 1 and type 2 diabetes. Many reports support the significant correlation between blood glucose level and peripheral insulin resistance. To determine the molecular mechanism underlying hyperglycemia-induced insulin resistance in skeletal muscles, post-receptor insulin-signaling events were assessed in skeletal muscles of neonatally streptozotocin-treated diabetic rats[39] and Zucker diabetic rats.[40] In soleus muscles isolated from diabetic rats, insulin-stimulated 2-deoxyglucose

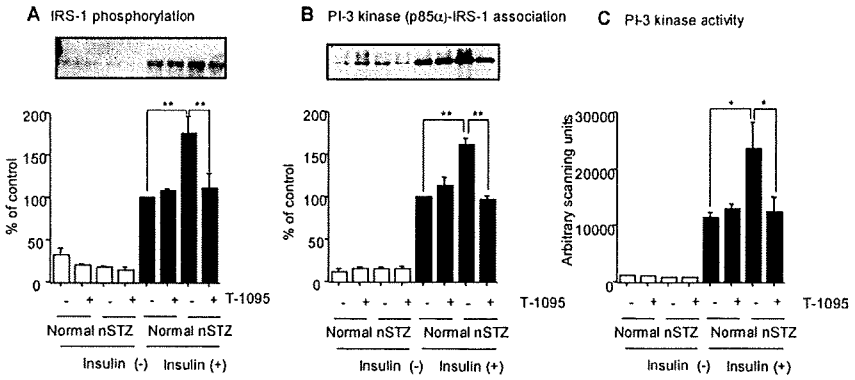

Fig. 4. Tyrosine Phosphorylation (A) of IRS-1, and Amount (p85α) (B) and Activity (C) of PI 3-kinase Associated with IRS-1 in Basal and Insulin-Stimulated Skeletal Muscle of Normal and nSTZ Rats with or without T-1095-Treatment

The proteins immunoprecipitated with anti-IRS-1 were subjected to SDS-PAGE followed by immunoblotting with anti-phosphorylated tyrosine (4G10) (A) or anti-p85α (B), or determination of PI 3-kinase activity (C). (A) A representative autoradiograph (upper) and the quantified data (lower) of tyrosine phosphorylation of IRS-1. (B) A representative autoradiograph (upper) and the quantified data (lower) of p85α associated with IRS-1. (C) PI 3-kinase activity associated with IRS-1. Results are expressed as the mean±S.E. for three animals. $*p<0.05$, $**p<0.01$.

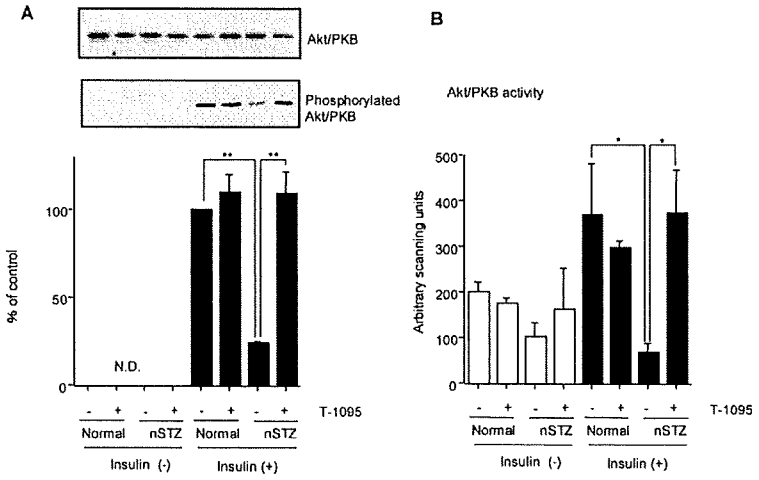

Fig. 5. The Protein Expression, Phosphorylation (Ser473) (A) and Activity (B) of Akt/PKB in Basal and Insulin-Stimulated Skeletal Muscle of Normal and nSTZ Rats with or without T-1095-Treatment

The total lysate was subjected to SDS-PAGE followed by immunoblotting with anti-Akt/PKB or anti-phosphorylated (Ser473) Akt/PKB (A). Equal amounts of muscle protein were immunoprecipitated with anti-Akt/PKB followed by determination of Akt/PKB activity (B). (A) Representative autoradiographs of Akt/PKB (upper) and phosphorylated Akt/PKB (middle), and the quantified data.

uptake, glucose oxidation and lactate release were all significantly decreased as compared with those of normal rats. Similarly, insulin-induced phosphorylation and activation of Akt/protein kinase B (PKB) and GLUT4 translocation were severely impaired. However, the upstream signals including phosphorylation of the insulin receptor and the insulin receptor substrate (IRS) -1/2, as well as PI 3-kinase activity associated with IRS-1/2, were enhanced. The amelioration of hyperglycemia by T-1095, a Na^+-glucose transporter inhibitor,[41] normalized the reduced insulin sensitivity in the soleus muscle, and the impaired insulin-stimulated Akt/PKB phosphorylation and activity. In addition, the enhanced PI 3-kinase activation and phosphorylation of the insulin receptor and IRS-1/2 were normalized. These results suggest that sustained hyperglycemia impairs the insulin-signaling steps between PI 3-kinase and Akt/PKB, and that impaired Akt/PKB activity underlies hyperglycemia-induced insulin resistance in skeletal muscle.

Salt-Sensitive or Angiotensin II-Related Hypertension Induces Insulin Resistance with Enhances in Insulin Signaling It is well-known that excessive salt intake elevates blood pressure and that hypertension often coexists with insulin resistance. However, the contribution of salt intake to the development of insulin resistance has yet to be clarified. We have investigated the molecular mechanism underlying insulin resistance in salt-sensitive rat models such as high-salt diet fed Sprague-Dawley rats,[42] Dahl salt-sensitive rats[43] and chronically angiotensin II (AII)-infused rats.[44] Importantly, the common observations in these rats were that despite that their being insulin-resistant, insulin-induced tyrosine phosphorylation of the insulin receptor and insulin receptor substrates, activation of phosphatidylinositol 3-kinase, and phosphorylation of Akt were all enhanced. Thus, the molecular mechanism underlying insulin resistance related to salt sensitive hypertension is unique, since many other factors causing insulin resistance such as obesity suppress an early insulin signaling step that is between the insulin receptor and PI 3-kinase activation. Interestingly, potassium (8%

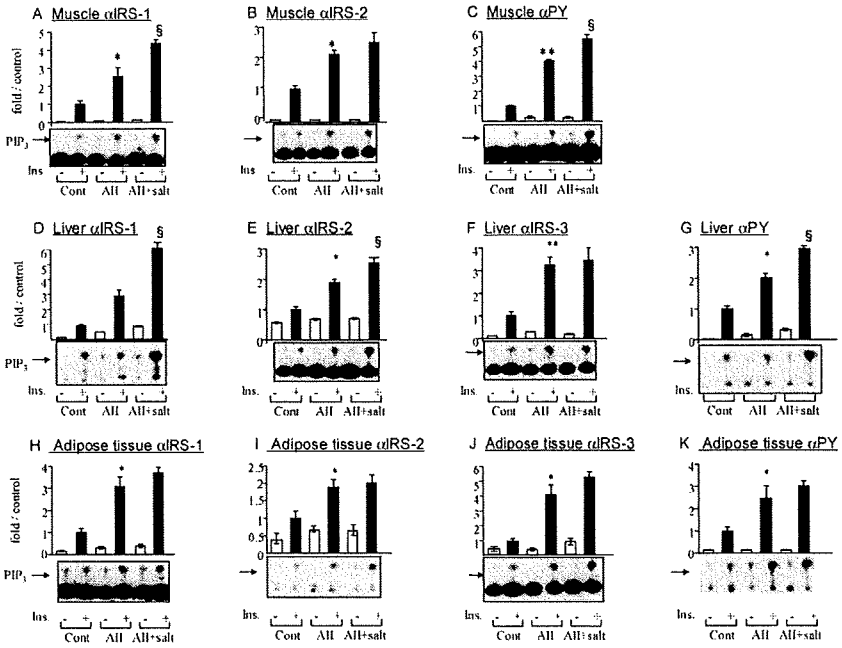

Fig. 6. Insulin-Stimulated PI 3-Kinase Activation in Skeletal Muscle, Liver and Fat of Angiotensin II-Infused Rats

Rats were anesthetized, and 4 ml of normal saline with or without 10^{-5} mol/l human insulin were then injected. Livers and hindlimb muscles were removed and homogenized (n=3 in each group). The lysates were subjected to immunoprecipitation with anti-IRS-1, anti-IRS-2, anti-IRS-3 or anti-phosphotyrosine antibodies followed by protein A-Sepharose 4FF. PI 3-kinase activities in the immunoprecipitates were assayed. The bar represents the average PI 3-kinase activity of three independently performed experiments. Representative spots of PI(3)P are shown. Data are means±S.E. $*p<0.05$ and $**p<0.01$ with the controls and $\S p<0.05$ compared with the AII group in the presence of insulin.

KCl) supplementation ameliorated the changes in insulin sensitivity in Dahl-S rats fed a high-salt diet, associated with a slight, but significant, decrease in blood pressure.

In addition, chronic AII infusion induced plasma cholesterylester hydroperoxide accumulation indicating increased oxidative stress, while treatment with tempol normalized plasma hydroperoxide levels in AII-infused rats. In addition, the tempol treatment normalized insulin resistance in AII-infused rats, as evidenced by a decreased glucose infusion rate in hyperinsulinemic euglycemic clamp study and decreased insulin-induced glucose uptake into isolated skeletal muscle, as well as enhanced insulin-induced PI 3-kinase activation as compared to the control rats. Thus, the mechanism underlying AII or high-salt diet induced insulin resistance may be increased oxidative stress, at least in part. Though further study is necessary to fully elucidate these mechanisms, our findings also suggest the importance of the development of new therapeutic approaches (for example, potassium supplementation or anti-oxidant administration) for patients with insulin resistance and hypertension.

REFERENCES

1) White M. F., Kahn C. R., *J. Biol. Chem.*, **269**, 1—4 (1994).
2) Ogihara T., Isobe T., Ichimura T., Taoka M., Funaki M., Sakoda H., Onishi Y., Inukai K., Anai M., Fukushima Y., Kikuchi M., Yazaki Y., Oka Y., Asano T., *J. Biol. Chem.*, **272**, 25267—25274 (1997).
3) Okada T., Kawano Y., Sakakibara T., Hazeki O., Ui M., *J. Biol. Chem.*, **269**, 3568—3573 (1994).
4) Katagiri H., Asano T., Ishihara H., Inukai K., Shibasaki Y., Kikuchi M., Yazaki Y., Oka Y., *J. Biol. Chem.*, **271**, 16987—16990 (1996).
5) Martin S. S., Haruta T., Morris A. J., Klippel A., Williams L. T., Olefsky J. M., *J. Biol. Chem.*, **271**, 17605—17608 (1996).
6) Gabbay R. A., Sutherland C., Gnudi L., Kahn B. B., O'Brien R. M., Granner D. K., Flier J. S., *J. Biol. Chem.*, **271**, 1890—1897 (1996).
7) Shepherd P. R., Nave B. T., Siddle K., *Biochem. Soc. Trans.*, **23**, 202S (1995).
8) Sutherland C., O'Brien R. M., Granner D. K., *J. Biol. Chem.*, **270**, 15501—15506 (1995).
9) Inoue G., Cheatham B., Emkey R., Kahn C. R., *J. Biol. Chem.*, **273**, 11548—11555 (1998).
10) Kido Y., Burks D. J., Withers D., Bruning J. C., Kahn C. R., White M. F., Accili D., *J. Clin. Invest.*, **105**, 199—205 (2000).
11) Songyang Z., Shoelson S. E., Chaudhuri M., Gish G., Pawson T., Haser W. G., King F., Roberts T., Ratnofsky S., Lechleider R. J., Neel B. G., Birge R. B., Fajardo J. E., Chou M. M., Hanafusa H., Schaffhausen B., Cantley L. C., *Cell*, **72**, 767—778 (1993).
12) Otsu M., Hiles I., Gout I., Fry M. J., Ruiz-Larrea F., Panayotou G., Thompson A., Dhand R., Hsuan J., Totty N., Smith A. D., Morgan S. J., Courtneidge S. A., Parker P. J., Waterfield M. D., *Cell*, **65**, 91—104 (1991).
13) Gout I., Dhand R., Panayotou G., Fry M. J., Hiles I., Otsu M., Waterfield M. D., *Biochem. J.*, **288**, 395—405 (1992).
14) Pons S., Asano T., Glasheen E., Miralpeix M., Zhang Y., Fisher T. L., Myers M. G., Sun X. J., White M. F., *Mol. Cell. Biol.*, **15**, 4453—4465 (1995).
15) Inukai K., Anai M., Breda E. V., Hosaka T., Katagiri H., Funaki M., Fukushima Y., Ogiwara T., Yazaki Y., Kikuchi M., Oka Y., Asano T., *J. Biol. Chem.*, **271**, 5317—5320 (1996).
16) Antonetti D., Algenstaedt P., Kahn C. R., *Mol. Cell. Biol.*, **16**, 2195—2203 (1996).
17) Inukai K., Funaki M., Ogihara T., Katagiri H., Kanda A., Anai M., Fukushima Y., Hosaka T., Suzuki M., Shin B. C., Takata K., Yazaki Y., Kikuchi M., Oka Y., Asano T., *J. Biol. Chem.*, **272**, 7873—7882 (1997).
18) Albert S., Twardzik T., Heisenberg M., Schneuwly S., *Gene*, **198**, 181—189 (1997).
19) Asano T., Kanda A., Katagiri H., Nawano M., Ogihara T., Inukai K., Anai M., Fukushima Y., Yazaki Y., Kikuchi M., Hooshmand-Rad R., Heldin C. H., Oka Y., Funaki M., *J. Biol. Chem.*, **275**, 17671—17676 (2000).
20) Stephens L., Anderson K., Stokoe D., Erdjument-Bromage H., Painter G. F., Holmes A. B., Gaffney P. R., Reese C. B., McCormick F., Tempst P., Coadwell J., Hawkins P. T., *Science*, **279**, 710—714 (1998).
21) Anderson K. E., Coadwell J., Stephens L. R., Hawkins P. T., *Curr.*

Biol., **8**, 684—691 (1998).
22) Singh S. S., Chauhan A., Brockerhoff H., Chauhan V. P., *Biochem. Biophys. Res. Commun.*, **195**, 104—112 (1993).
23) Klarlund J. K., Guilherme A., Holik J. J., Virbasius J. V., Chawla A., Czech M. P., *Science*, **275**, 1927—1930 (1997).
24) Venkateswarlu K., Oatey P. B., Tavare J. M., Cullen P. J., *Curr. Biol.*, **8**, 463—466 (1998).
25) Rameh L. E., Arvidsson A. K., Carraway K. L., 3rd., Couvillon A. D., Rathbun G., Crompton A., VanRenterghem B., Czech M. P., Ravichandran K. S., Burakoff S. J., Wang D. S., Chen C. S., Cantley L. C., *J. Biol. Chem.*, **272**, 22059—22066 (1997).
26) Sander E. E., van Delft S., ten Klooster J. P., Reid T., van der Kammen R. A., Michiels F., Collard J. G., *J. Cell. Biol.*, **143**, 1385—1398 (1998).
27) Rameh L. E., Chen C. S., Cantley L. C., *Cell*, **83**, 821—830 (1995).
28) Salim K., Bottomley M. J., Querfurth E., Zvelebil M. J., Gout I., Scaife R., Margolis R. L., Gigg R., Smith C. I., Driscoll P. C., Waterfield M. D., Panayotou G., *EMBO J.*, **15**, 6241—6250 (1996).
29) Bae Y. S., Cantley L. G., Chen C. S., Kim S. R., Kwon K. S., Rhee S. G., *J. Biol. Chem.*, **273**, 4465—4469 (1998).
30) Lambrechts A., Verschelde J. L., Jonckheere V., Goethals M., Vandekerckhove J., Ampe C., *EMBO J.*, **16**, 484—494 (1998).
31) Alessi D. R., James S. R., Downes C. P., Holmes A. B., Gaffney P. R., Reese C. B., Cohen P., *Curr. Biol.*, **7**, 261—269 (1997).
32) Sarbassov D. D., Guertin D. A., Ali S. M., Sabatini D. M., *Science*, **307**, 1098—1101 (2005).
33) Whiteman E. L., Cho H., Birnbaum M. J., *Trends Endocrinol. Metab.*, **13**, 444—451 (2002).
34) Cho H., Mu J., Kim J. K., Thorvaldsen J. L., Cho Q., Crensshaw E. B., 3rd., Kaestner K. H., Bartlomei M. S., Shulman G. I., Birnbaum M. J., *Science*, **292**, 1728—1731 (2001).
35) Hotamisligil G. S., Budavari A., Murray D., Spiegelman B. M., *J. Clin. Invest.*, **94**, 1543—1549 (1994).
36) Anai M., Funaki M., Ogihara T., Terasaki J., Inukai K., Katagiri H., Fukushima Y., Yazaki Y., Kikuchi M., Oka Y., Asano T., *Diabetes*, **47**, 13—23 (1998).
37) Anai M., Funaki M., Ogihara T., Kanda A., Onishi Y., Sakoda H., Inukai K., Nawano M., Fukushima Y., Yazaki Y., Kikuchi M., Oka Y., Asano T., *Diabetes*, **48**, 158—169 (1999).
38) Folli F., Saad M. J., Backer J. M., Kahn C. R., *J. Clin. Invest.*, **92**, 1787—1794 (1993).
39) Nawano M., Ueta K., Oku A., Arakawa K., Saito A., Funaki M., Anai M., Kikuchi M., Oka Y., Asano T., *Biochem. Biophys. Res. Commun.*, **266**, 252—256 (1999).
40) Nawano M., Oku A., Ueta K., Umebayashi I., Ishirahara T., Arakawa K., Saito A., Anai M., Kikuchi M., Asano T., *Am. J. Physiol. Endocrinol. Metab.*, **278**, E535—E543 (2000).
41) Oku A., Ueta K., Arakawa K., Ishihara T., Nawano M., Kuronuma Y., Matsumoto M., Saito A., Tsujihara K., Anai M., Asano T., Kanai Y., Endou H., *Diabetes*, **48**, 1794—1800 (1999).
42) Ogihara T., Asano T., Ando K., Chiba Y., Sekine N., Sakoda H., Anai M., Onishi Y., Fujishiro M., Ono H., Shojima N., Inukai K., Fukushima Y., Kikuchi M., Fujita T., *Diabetes*, **50**, 573—583 (2001).
43) Ogihara T., Asano T., Ando K., Sakoda H., Anai M., Shojima N., Ono H., Onishi Y., Fujishiro M., Abe M., Fukushima Y., Kikuchi M., Fujita T., *Hypertension*, **40**, 83—89 (2002).
44) Ogihara T., Asano T., Ando K., Chiba Y., Sakoda H., Anai M., Shojima N., Ono H., Onishi Y., Fujishiro M., Katagiri H., Fukushima Y., Kikuchi M., Noguchi N., Aburatani H., Komuro I., Fujita T., *Hypertension*, **40**, 872—879 (2002).

ELSEVIER

Atherosclerosis 196 (2008) 391–397

ATHEROSCLEROSIS

www.elsevier.com/locate/atherosclerosis

A novel method for evaluating human carotid artery elasticity: Possible detection of early stage atherosclerosis in subjects with type 2 diabetes

Hisashi Okimoto [a,1], Yasushi Ishigaki [a,1], Yoshihiro Koiwa [b], Yoshinori Hinokio [a], Takehide Ogihara [c], Susumu Suzuki [a], Hideki Katagiri [c,f], Takayoshi Ohkubo [d,f], Hideyuki Hasegawa [e], Hiroshi Kanai [e], Yoshitomo Oka [a,g,*]

[a] *Division of Molecular Metabolism and Diabetes, Tohoku University Graduate School of Medicine, Japan*
[b] *Division of Cardiovascular Medicine, Tohoku University Graduate School of Medicine, Japan*
[c] *Division of Advanced Therapeutics for Metabolic Diseases, Tohoku University Graduate School of Medicine, Japan*
[d] *Department of Planning for Drug Development and Clinical Evaluation, Tohoku University Graduate School of Pharmaceutical Science and Medicine, Japan*
[e] *Department of Electrical Engineering, Tohoku University Graduate School of Engineering, Japan*
[f] *The 21st Century COE Programs, Comprehensive Research and Education Center for Planning of Drug Development and Clinical Evaluation, Japan*
[g] *The 21st Century COE Programs, Center for Innovative Therapeutic Development towards the Conquest of Signal Transduction Diseases, Tohoku University, Sendai, Japan*

Received 29 March 2006; received in revised form 5 September 2006; accepted 12 November 2006
Available online 18 December 2006

Abstract

We recently developed a novel method for evaluating the elasticity of arterial walls, the phased tracking method. Herein, we evaluated atherosclerosis of the carotid artery with this method in 242 individuals with type 2 diabetes. In multiple regression analysis of subject status, age, systolic blood pressure and hyperlipidemia were found to be independently associated with carotid artery elasticity values. We also measured currently established values for atherosclerosis, carotid artery IMT and baPWV, in these subjects. Carotid artery elasticity correlated with max IMT ($r=0.291$, $p<0.01$), plaque score (PS) ($r=0.220$, $p<0.01$) and baPWV ($r=0.345$, $p<0.01$). Elasticity, max IMT and plaque score, all correlated with the number of risk factors for atherosclerosis, i.e. hypertension, hyperlipidemia and smoking, in addition to diabetes, consistent with the view that these values reflect atherosclerosis. Importantly, however, in subjects with IMT <1.1 mm, who are classified as not having atherosclerosis as defined by IMT criteria, only carotid artery elasticity correlated with the number of risk factors ($p<0.05$). These results suggest that (1) the measured carotid artery elasticity values reflect atherosclerosis and (2) our novel method has potential for detecting atherosclerosis in its early stage.

Keywords: Human carotid artery elasticity; Atherosclerosis; Diabetes

1. Introduction

Individuals with type 2 diabetes are at very high risk for atherosclerosis [1]. Although many methods have been developed for detecting atherosclerosis, those currently available are mainly for detecting established atherosclerosis. Therefore, the disease process is well-advanced at the time of diagnosis. To reduce future cardiovascular complications in subjects with atherogenic disorders such as type 2 diabetes

* Corresponding author at: Division of Molecular Metabolism and Diabetes, Tohoku University Graduate School of Medicine, 2-1 Seiryo-machi, Aoba-ku, Sendai 980-8575, Japan. Tel.: +81 22 717 7611; fax: +81 22 717 7611.
E-mail address: oka-y@mail.tains.tohoku.ac.jp (Y. Oka).
[1] These authors contributed equally to this work.

0021-9150/$ – see front matter © 2006 Elsevier Ireland Ltd. All rights reserved.
doi:10.1016/j.atherosclerosis.2006.11.020

mellitus, detection of early stage atherosclerosis is urgently needed.

Carotid intima-media thickness (IMT) is a well-established surrogate marker for cardiovascular risk [2]. Measuring IMT with ultrasonography is non-invasive and relatively simple [3,4], and IMT is now commonly employed as an endpoint marker in clinical trials. Carotid IMT correlates with cardiovascular risk factors and indeed predicts macrovascular events such as myocardial infarction [5] and stroke [6]. Carotid IMT is greater in subjects with diabetes, both type 1 [7] and type 2 [8,9], than in non-diabetic subjects of the same age. When analyzed in diabetic patients, IMT correlates with glycemic control and the duration of diabetes. Interventions, such as blood glucose lowering [10], lipid lowering [11], ACE inhibition [12] and anti-platelet treatment [13], have been demonstrated to suppress IMT progression. However, it has also been reported that IMT is not affected by either therapeutic interventions [14] or glycemic control [15]. These conflicting results might be attributable to a very small change in IMT, a 0.1 mm increase per decade in normal subjects. Such a small change may mask actual change due to inter-assay variations in IMT measurement. Most importantly, it is not possible to make a diagnosis of atherosclerosis until the appearance of arterial wall thickening.

We recently developed a novel non-invasive method for evaluating the movement of multiple sites in cardiac and arterial walls (3.616 measurement sites/9.0 mm × 6.4 mm) during a single heartbeat [16,17]. This innovative phased tracking method enables us to evaluate regional characteristics; the softer the site, the more easily it deforms during one heartbeat. This reflects regional elasticity. This method has already been applied to the in vivo detection of regional changes in cardiac and arterial walls [18–20], and the interventricular septum [21]. Evaluation of plaque vulnerability has also been attempted [16]. It is theoretically possible to detect qualitative changes in the carotid arterial wall with this method. We therefore tested the possibility of being able to detect atherosclerosis in the early stage.

Herein, we show that carotid artery elasticity, as measured in Japanese subjects with type 2 diabetes, correlates well with results obtained with currently established methods for evaluating atherosclerosis. Most importantly, elasticity correlates with the number of risk factors for atherosclerosis in those with IMT <1.1 mm, who are classified as not having atherosclerosis as defined by IMT criteria [22,23]. These results strongly suggest that it is possible to detect early stage atherosclerosis with this novel method.

2. Methods

2.1. Study subjects

The study subjects were recruited from among patients followed at the diabetes clinic at Tohoku University Hospital. Patients with type 1 diabetes, renal failure (serum creatinine >2.0 mg/dl), severe heart failure (NYHA functional class 2–4), atrial fibrillation and peripheral arterial disease were excluded from the study. All participants analyzed were Japanese type 2 diabetes patients ($n=242$) who met the WHO criteria for diabetes mellitus. The study protocol was approved by the Tohoku University Institutional Review Board. Informed consent was obtained from each patient. Subjects characteristics are shown in Table 1.

Table 1
Subject characteristics

Number	242
Age (years)	62.1 ± 12.4
Male (%)	54.1
Body weight (kg)	62.2 ± 13.6
BMI (kg/m^2)	24.2 ± 4.2
Duration of diabetes (years)	12.0 ± 9.70
Fasting blood glucose (mg/dl)	141 ± 32.1
HbA1c (%)	7.08 ± 1.33
Systolic blood pressure (mmHg)	130 ± 18.3
Diastolic blood pressure (mmHg)	75.8 ± 11.1
Total cholesterol (mg/dl)	191 ± 38.4
HDL cholesterol (mg/dl)	51.2 ± 14.6
LDL cholesterol (mg/dl)	115 ± 31.9
Triglyceride (mg/dl)	127 ± 94.1
Uric acid (mg/dl)	5.09 ± 1.37
High-sensitive CRP (mg/dl)	0.18 ± 0.23
Diabetic retinopathy (%)	30.2
Microalbumiuria or proteinuria (%)	38.8
Diabetic neuropathy (%)	46.4
Diet:OHA:insulin (%)	20.0:37.8:42.2
Hyperlipidemia (%)	37.2
Hypertension (%)	39.3
Current smoker (%)	30.6
BMI >25 (%)	38.0

Data are presented as means ± S.D.

We used the following criteria for atherogenic risk factors. Hyperlipidemia was defined as total cholesterol ≥5.7 mmol/dl (220 mg/dl) and/or triglyceride ≥1.7 mmol/l (150 mg/dl), based on the definition proposed by the Japan Atherosclerosis Society in 2002, or taking antihyperlipidemic drugs. The subjects whose systolic BP ≥140 mmHg and/or diastolic BP ≥90 mmHg (The Japanese Society of Hypertension guidelines in 2004) or who were taking antihypertensive drugs were defined as having hypertension. The subjects who currently smoked were classified as current smokers.

2.2. Measurement of ABI and baPWV

Ankle brachial pressure index (ABI) and brachial ankle pulse wave velocity (baPWV) were measured using an automatic waveform analyzer (BP-203RPE; Colin Co., Komaki, Japan) after a 5 min rest. This device was designed to simultaneously measure blood pressure levels in both arms (brachial arteries) and ankles (posterior tibial arteries), and to then calculate the ankle systolic BP/brachial systolic BP. Pulse waves were recorded on the right brachial artery and both posterior tibial arteries. The average baPWV was calculated by divid-

ing the arm–ankle distance by the pulse wave transmission time between these points.

2.3. Measurement of carotid artery intima-media thickness

Intima-media thickness of the carotid arteries was measured using ultrasound diagnostic equipment (EUB-450, Hitachi Medico, Tokyo, Japan) with an electrical linear transducer (mid-frequency of 7.5 MHz). The common carotid artery (CCA), carotid bulb and portions of the internal and external carotid arteries on both sides were scanned with the subject in the supine position. The scan encompasses the region between 30 mm proximal to the beginning of the dilation of the bifurcation bulb and 15 mm distal to the CCA flow divider. We defined the max IMT as the thickest IMT in the scanned regions [24] and a max IMT <1.1 mm was considered normal. We defined a plaque, a focal IMT thickening, as an area with IMT ≥1.1 mm and calculated the plaque score (PS) by totaling the maximal thickness values of all plaques in the scanned area [25]. The scans were performed by a trained sonographer and the scanning period averaged 20 min in each patient.

2.4. Measurement of arterial wall elasticity

Real-time measurement of regional elasticity in the carotid artery wall was achieved based on a previously described method [20] with ultrasound diagnostic equipment (prototype system by Panasonic). With this system, an ultrasound beam is used for sequential scanning at 32 positions with a linear type 7.5 MHz probe. Multiple points were preset from the luminal surface to the adventitia along each beam with constant intervals of 320 μm, and multiple layers were defined as being between two neighboring points. Then, the displacement of each point preset along each beam was obtained by applying the phased tracking method to the received echo. Minute changes in the thickness of each layer were determined by subtracting displacements of two neighboring points. The elasticity of each layer was obtained from the thickness change and the blood pressure measured at the upper arm. Since the reflected ultrasound was resampled at an interval of 107 ns (=80 μm along the depth direction) after quadrature demodulation, we further divided each layer with a thickness of 320 μm into four points, shifted the initial depth of each layer by one-fourth of 320 μm, and applied the above procedure to each depth. Thus, the elasticity was obtained at intervals of 80 μm in the depth direction and 200 μm in the axial direction of the artery. A cross-sectional image and the process of elasticity measurement are schematically depicted in Fig. 1.

2.5. Statistical analysis

Variables were compared using Pearson's regression analysis and Student's *t*-test as appropriate. Then, a multiple linear regression analysis was performed to evaluate the independent parameters that were significantly related to arterial elasticity. The relationships between number of risk factors and the values of atherosclerosis markers were examined by analysis of covariance (ANCOVA), adjusted with age as a covariate. A p value less than 0.05 was accepted as indicating statistical significance. All statistical analyses were performed using the Statistical Package for the Social Sciences Version 13.0 (SPSS Japan Inc., Tokyo, Japan).

3. Results

We assessed the associations of carotid artery elasticity with subject characteristics (Table 2). Elasticity correlated

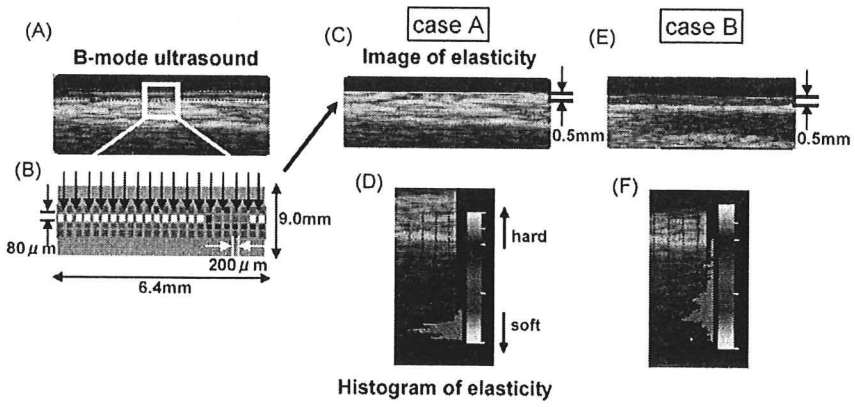

Fig. 1. The intima–media complex was visualized by conventional B-mode scanning (A), and minute thickness changes in the layers at each depth (113 depths × 32 beams per 9 mm × 6.4 mm scanned area) during one heart beat were then recorded by the phased tracking method (B). Thickness changes in each layer represent deformity, a reflection of elasticity. This elasticity is displayed as a 2D cross-sectional color image on B-mode scanning, and the image is updated at every heartbeat (C). The elasticity distribution is shown as a histogram (D). Representative results obtained from a normal subject, case A (male, age 40), are shown. Case B (male, age 45), in marked contrast, suffered from type 2 diabetes, hyperlipidemia and an old cerebral infarction, but had an IMT of only 0.5 mm, the same thickness as that of case A. The elasticity (E) was, however, extremely different from that of case A, as shown in the histogram (F).

Table 2
Associations between arterial elasticity and subject characteristics

Variables	r-Value	p-Value
Age	0.34	<0.01
Duration of diabetes	0.136	<0.05
Fasting blood glucose	−0.012	0.86
HbA1c	−0.003	0.97
Total cholesterol	0.103	0.10
HDL cholesterol	0.066	0.31
LDL cholesterol	0.089	0.17
Triglyceride	−0.064	0.32
Systolic blood pressure	0.443	<0.01
Diastolic blood pressure	0.147	<0.05
Uric acid	−0.03	0.65
High-sensitive CRP	0.037	0.56

Table 3
Mean arterial elasticity values in the presence and absence of cardiovascular risk factors

Variables	Elasticity (kPa)		p
	−	+	
Male	51.6 ± 12.6	51.0 ± 14.5	0.99
Hyperlipidemia	49.8 ± 12.3	54.7 ± 13.7	<0.01
Hypertension	49.6 ± 13.3	54.8 ± 13.6	<0.01
Current smoker	51.6 ± 13.3	51.8 ± 14.5	0.88
BMI >25	51.6 ± 13.7	51.6 ± 13.5	0.99
Diabetic retinopathy	52.3 ± 13.7	50.9 ± 14.1	0.67
Diabetic nephropathy	50.5 ± 13.6	53.9 ± 13.6	0.06
Diabetic neuropathy	50.8 ± 12.9	51.4 ± 14.4	0.65

Data are presented as means ± S.D.

Table 4
Multivariate adjustment for parameters related to arterial elasticity

Variables	Coefficient (β)	95% CI	p-Value
Age (years)	0.28	0.18–0.43	<0.01
Duration of diabetes (years)	−0.02	−0.18–0.14	0.77
Systolic blood pressure (mmHg)	0.39	0.21–0.38	<0.01
Hyperlipidemia	0.11	0.08–6.24	<0.05

with age ($r = 0.340$, $p < 0.01$), duration of diabetes ($r = 0.136$, $p < 0.05$) and blood pressure, both systolic ($r = 0.430$, $p < 0.01$) and diastolic ($r = 0.147$, $p < 0.05$).

We then examined whether or not cardiovascular risk factors affect arterial elasticity values (Table 3). Hyperlipidemic subjects had significantly higher arterial elasticity values than those with normal lipid profiles. Similarly, subjects with hypertension had higher values. However, arterial elasticity values did not depend on other risk factors, such as sex, obesity, smoking and diabetic complications.

To elucidate the independent variables affecting arterial elasticity, we performed multiple linear regression analysis with parameters related to elasticity. We employed four clinical parameters, age, duration of diabetes, systolic blood pressure and hyperlipidemia, based on the results shown in Tables 2 and 3. We found age, systolic blood pressure and hyperlipidemia to be independently associated with elasticity values (Table 4).

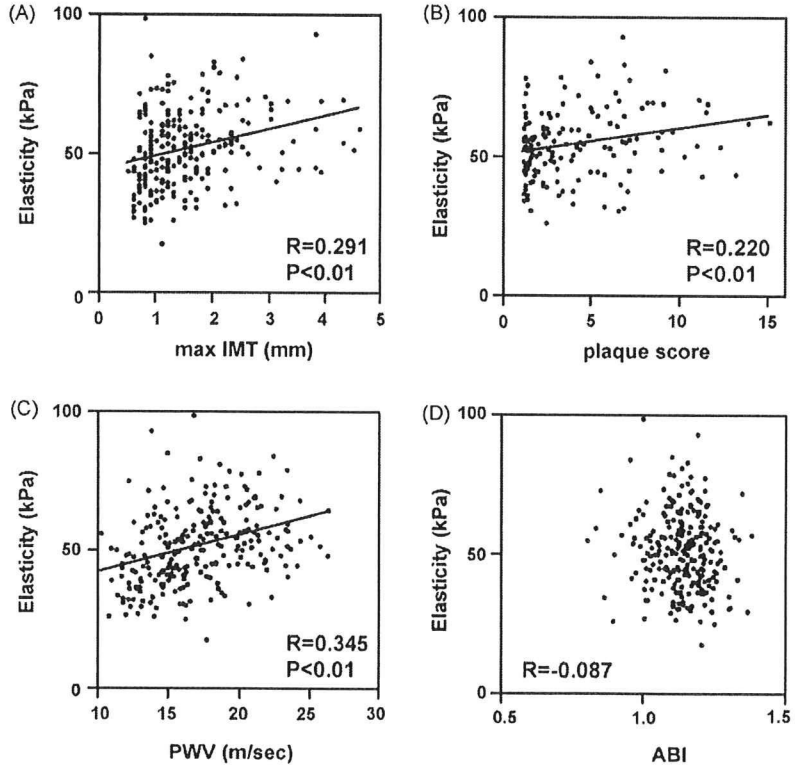

Fig. 2. Correlations between arterial elasticity values and max IMT (A), plaque score (B), baPWV (C) and ABI (D).

To assess the clinical relevance of carotid artery elasticity, we compared our elasticity values to those obtained with currently established methods for evaluating atherosclerosis: max IMT, plaque score, baPWV and ABI. Carotid artery elasticity showed significant positive correlations with max IMT ($r=0.291$, $p<0.01$) (Fig. 2A), the plaque score ($r=0.220$, $p<0.01$, $n=160$) (Fig. 2B) and baPWV ($r=0.345$, $p<0.01$) (Fig. 2C) in subjects with type 2 diabetes. It should be kept in mind that the plaque score can be obtained only in subjects with IMT ≥ 1.1 mm ($n=160$), such that the correlation was studied only in those having definite atherosclerosis based on IMT criteria [22,23]. Arterial elasticity showed no correlation with the ABI value ($r=-0.087$, $p=0.176$) (Fig. 2D). However, when we performed multiple linear regression analysis adjusted with independent parameters, age, systolic blood pressure and hyperlipidemia (Table 4), the correlations between elasticity and atherosclerosis markers (max IMT, plaque score and baPWV) were no longer present.

In a subject with more than one risk factor, the atherosclerotic process would be accelerated and thus affect the values of atherosclerosis markers. Four modifiable risk factors, diabetes, hypertension, hyperlipidemia and current smoking,

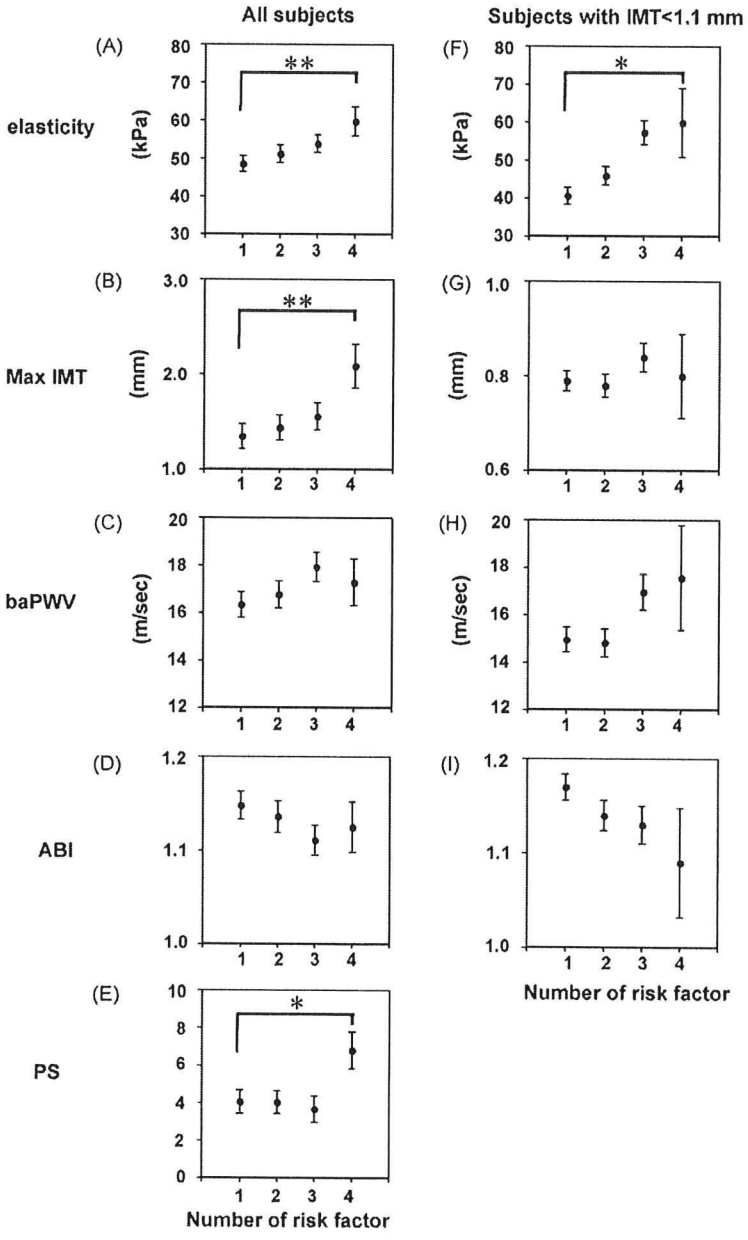

Fig. 3. Correlations of values reflecting atherosclerosis with the number of risk factors in all study subjects (A–E, $n=242$) and subjects with max IMT <1.1 mm (F–I, $n=82$). Data are presented as means ± S.E. $^{*}p<0.05$, $^{**}p<0.01$.

were taken into account in this study. All subjects had at least one risk factor, diabetes. When all the subjects were analyzed by ANCOVA, adjusted with age as a covariate, the higher the number of risk factors, the greater the attenuation of arterial elasticity values, max IMT and the plaque score (Fig. 3A, B, E). However, very interestingly, when subjects with max IMT <1.1 mm, who are regarded as not having atherosclerosis based on IMT criteria, were analyzed ($n = 82$), only age-adjusted carotid artery elasticity correlated with an increasing number of risk factors (Fig. 3F). Other age-adjusted parameters for evaluating atherosclerosis, max IMT, baPWV and ABI, showed no significant correlations with a greater number of risk factors in subjects with max IMT <1.1 mm (Fig. 3G–I).

4. Discussions

Our most important finding is that in subjects with max IMT <1.1 mm, who are regarded as being free of atherosclerosis based on IMT criteria [22,23], only carotid artery elasticity as measured with our novel non-invasive method correlated with an increasing number of risk factors. No other values obtained with the currently available methods showed correlations with the number of risk factors in these "non-atherosclerotic" subjects. Thus, our novel method of measuring arterial wall elasticity raises the possibility of detecting atherosclerosis in its early stage.

Carotid artery elasticity correlates well with results obtained with currently established methods for evaluating atherosclerosis in subjects with type 2 diabetes. These results strongly suggest that elasticity as measured with our current method reflects the severity of atherosclerosis. The measurement procedures are relatively simple, essentially the same as those of B-mode ultrasonography. In addition, arterial wall elasticity is shown as a color coded cross-sectional image with a side by side B-mode ultrasonogram, which is very practical in the clinical setting.

This novel ultrasonic method accurately tracks the movement of the arterial wall based on both the phase and the magnitude of demodulated signals, allowing instantaneous determination of the position of an object. With this method, it is possible to accurately detect small-amplitude velocity signals, less than a few micrometers, that are superimposed on arterial wall motion due to the heartbeat. This method thus allows the elasticity, a qualitative feature, of the arterial wall to be evaluated. In addition to detecting the early stage atherosclerosis, this method may enable us to evaluate progression or regression of atherosclerosis in a much shorter time than currently available methods. This possibility is extremely interesting because a means of evaluating whether or not a treatment is effective for preventing atherosclerosis is urgently needed. It usually takes years to detect the progression or regression of atherosclerosis, while it may take only months with our present method of qualitative arterial wall measurement. For example, it may be possible to detect an improvement in response to statin treatment within a few months. Similarly, we will be able to assess the effects on atherosclerosis of altering risk factors within months. These possibilities clearly merits further study.

A variety of methods are widely used for evaluating atherosclerosis. Measuring carotid IMT with ultrasound is one of the most well-established methods because it is safe, non-invasive, reproducible and easy to perform. IMT provides quantitative information, i.e. vessel-wall thickness. Depicting changes in IMT is thus generally thought to take a long time. baPWV is also a non-invasive method, which assesses atherosclerosis, as a reflection of arterial stiffness, and the usefulness of baPWV has been reported in clinical studies [26–28]. However, the pulse wave velocity depends on the ratio of the inner radius of the artery to wall thickness, which is not related to regional elasticity. It also reportedly depends on heart rate [29].

While the elasticity average of the intima and media of the carotid artery wall was calculated and used for evaluation of atherosclerosis in this study, another interesting aspect of elasticity is its distribution. The elasticity distribution, which is depicted in a histogram, might provide additional information regarding qualitative changes in atherosclerosis, and should be comprehensively studied in the future. In conclusion, our novel method for evaluating carotid artery wall elasticity holds promise for early detection of atherosclerosis.

Acknowledgments

This work was supported by a Grant-in-Aid for Scientific Research (17790599) to Y. Ishigaki and the 21st Century COE Programs "Innovative Therapeutic Development towards the Conquest of Signal Transduction Diseases" to Y. Oka from the Ministry of Education, Science, Sports and Culture of Japan. This work was also supported by a Grant-in-Aid for Research on Human Genome, Tissue Engineering (H17-genome-003) to Y. Oka. We thank Healthcare Business Company, Matsushita Electric Industrial Co., Ltd. (Panasonic), Yokohama, Japan for supplying the prototype elasticity measurement system for this study.

References

[1] Kannel WB, McGee DL. Diabetes and cardiovascular disease. The Framingham study. JAMA 1997;241:2035–8.
[2] O'Leary DH, Polak JF, Kronmal RA, et al. Carotid-artery intima and media thickness as a risk factor for myocardial infarction and stroke in older adults. Cardiovascular Health Study Collaborative Research Group. N Engl J Med 1999;340:14–22.
[3] Pignoli P, Tremoli E, Poli A, Oreste P, Paoletti R. Intimal plus medial thickness of the arterial wall: a direct measurement with ultrasound imaging. Circulation 1986;74:1399–406.
[4] Salonen JT, Korpela H, Salonen R, Nyyssonen K. Precision and reproducibility of ultrasonographic measurement of progression of common carotid artery atherosclerosis. Lancet 1993;341:1158–9.

[5] Bots ML, Hoes AW, Koudstaal PJ, Hofman A, Grobbee DE. Common carotid intima-media thickness and risk of stroke and myocardial infarction: the Rotterdam Study. Circulation 1997;96:1432–7.
[6] Touboul PJ, Elbaz A, Koller C, et al. Common carotid artery intima-media thickness and brain infarction: the Etude du Profil Genetique de l'Infarctus Cerebral (GENIC) case-control study. The GENIC Investigators. Circulation 2000;102:313–8.
[7] Yamasaki Y, Kawamori R, Matsushima H, et al. Atherosclerosis in carotid artery of young IDDM patients monitored by ultrasound high-resolution B-mode imaging. Diabetes 1994;43:634–9.
[8] Folsom AR, Eckfeldt JH, Weitzman S, et al. Relation of carotid artery wall thickness to diabetes mellitus, fasting glucose and insulin, body size, and physical activity. Atherosclerosis Risk in Communities (ARIC) Study Investigators. Stroke 1994;25:66–73.
[9] Kawamori R, Yamasaki Y, Matsushima H, et al. Prevalence of carotid atherosclerosis in diabetic patients. Ultrasound high-resolution B-mode imaging on carotid arteries. Diabetes Care 1992;15:1290–4.
[10] Minamikawa J, Tanaka S, Yamauchi M, Inoue D, Koshiyama H. Potent inhibitory effect of troglitazone on carotid arterial wall thickness in type 2 diabetes. J Clin Endocrinol Metab 1998;83:1818–20.
[11] Furberg CD, Adams Jr HP, Applegate WB, et al. Effect of lovastatin on early carotid atherosclerosis and cardiovascular events. Asymptomatic Carotid Artery Progression Study (ACAPS) Research Group. Circulation 1994;90:1679–87.
[12] Lonn E, Yusuf S, Dzavik V, et al. Effects of ramipril and Vitamin E on atherosclerosis: the study to evaluate carotid ultrasound changes in patients treated with ramipril and Vitamin E (SECURE). Circulation 2001;103:919–25.
[13] Kodama M, Yamasaki Y, Sakamoto K, et al. Antiplatelet drugs attenuate progression of carotid intima-media thickness in subjects with type 2 diabetes. Thromb Res 2000;97:239–45.
[14] Beishuizen ED, van de Ree MA, Jukema JW, et al. Two-year statin therapy does not alter the progression of intima-media thickness in patients with type 2 diabetes without manifest cardiovascular disease. Diabetes Care 2004;27:2887–92.
[15] Rantala AO, Paivansalo M, Kauma H, et al. Hyperinsulinemia and carotid atherosclerosis in hypertensive and control subjects. Diabetes Care 1998;21:1188–93.
[16] Kanai H, Hasegawa H, Ichiki M, Tezuka F, Koiwa Y. Elasticity imaging of atheroma with transcutaneous ultrasound: preliminary study. Circulation 2003;107:3018–21.
[17] Hasegawa H, Kanai H, Hoshimiya N, Koiwa Y. Evaluating the regional elastic modules of a cylindrical shell with nonuniform wall thickness. J Med Ultrason 2004;31:81–90.
[18] Kanai H, Sato M, Koiwa Y, Chubachi N. Transcutaneous measurement and spectrum analysis of heart wall vibrations. IEEE Trans Ultrason Ferroelectr Freq Control 1996;43:791–810.
[19] Kanai H, Koiwa Y, Zhang J. Real-time measurement of local myocardium motion and arterial wall thickening. IEEE Trans Ultrason Ferroelectr Freq Control 1999;46:1229–41.
[20] Hasegawa H, Kanai H, Hoshimiya N, Chubachi N, Koiwa Y. Accuracy evaluation in the measurement of a small change in the thickness of arterial walls and the measurement of elasticity of the human carotid artery. Jpn J Appl Phys 1998;37:3101–5.
[21] Kanai H, Hasegawa H, Chubachi N, Koiwa Y, Tanaka M. Noninvasive evaluation of local myocardinal thickening and its color-coded imaging. IEEE Trans Ultrason Ferroelectr Freq Control 1997;44:752–68.
[22] Salonen R, Seppanen K, Rauramaa R, Salonen JT. Prevalence of carotid atherosclerosis and serum cholesterol levels in eastern Finland. Arteriosclerosis 1988;8:788–92.
[23] Poli A, Tremoli E, Colombo A, et al. Ultrasonographic measurement of the common carotid artery wall thickness in hypercholesterolemic patients. A new model for the quantitation and follow-up of preclinical atherosclerosis in living human subjects. Atherosclerosis 1988;70:253–61.
[24] O'Leary DH, Polak JF, Kronmal RA, et al. Distribution and correlates of sonographically detected carotid artery disease in the Cardiovascular Health Study. The CHS Collaborative Research Group. Stroke 1992;23:1752–60.
[25] Handa N, Matsumoto M, Maeda H, et al. Ultrasonic evaluation of early carotid atherosclerosis. Stroke 1990;21:1567–72.
[26] Lehmann ED, Hopkins KD, Gosling RG. Increased aortic stiffness in women with NIDDM. Diabetologia 1996;39:870–1.
[27] Farrar DJ, Green HD, Wagner WD, Bond MG. Reduction in pulse wave velocity and improvement of aortic distensibility accompanying regression of atherosclerosis in the rhesus monkey. Circ Res 1980;47:425–32.
[28] Lehmann ED, Riley WA, Clarkson P, Gosling RG. Non-invasive assessment of cardiovascular disease in diabetes mellitus. Lancet 1997;350(Suppl. 1):SI14–9.
[29] Lantelme P, Mestre C, Lievre M, Gressard A, Milon H. Heart rate: an important confounder of pulse wave velocity assessment. Hypertension 2002;39:1083–7.

Am J Physiol Endocrinol Metab 294: E719–E725, 2008.
First published February 12, 2008; doi:10.1152/ajpendo.00253.2007.

Hepatic overexpression of a dominant negative form of raptor enhances Akt phosphorylation and restores insulin sensitivity in K/KAy mice

Yuko Koketsu,[1] Hideyuki Sakoda,[1] Midori Fujishiro,[1] Akifumi Kushiyama,[1] Yasushi Fukushima,[1] Hiraku Ono,[1] Motonobu Anai,[2] Takako Kikuchi,[1] Takeshi Fukuda,[1] Hideaki Kamata,[4] Nanao Horike,[3] Yasunobu Uchijima,[3] Hiroki Kurihara,[3] and Tomoichiro Asano[4]

[1]*Department of Internal Medicine, Graduate School of Medicine, University of Tokyo;* [2]*Institute for Adult Disease, Asahi Life Foundation;* [3]*Department of Physiological Chemistry and Metabolism, Graduate School of Medicine, University of Tokyo, Tokyo; and* [4]*Department of Medical Science, Graduate School of Medicine, University of Hiroshima, Hiroshima, Japan*

Submitted 28 August 2007; accepted in final form 11 February 2008

Koketsu Y, Sakoda H, Fujishiro M, Kushiyama A, Fukushima Y, Ono H, Anai M, Kikuchi T, Fukuda T, Kamata H, Horike N, Uchijima Y, Kurihara H, Asano T. Hepatic overexpression of a dominant negative form of raptor enhances Akt phosphorylation and restores insulin sensitivity in K/KAy mice. *Am J Physiol Endocrinol Metab* 294: E719–E725, 2008. First published February 12, 2008; doi:10.1152/ajpendo.00253.2007.—Several serine/threonine kinases reportedly phosphorylate serine residues of IRS-1 and thereby induce insulin resistance. In this study, to investigate the effect of mTOR/raptor on insulin signaling and metabolism in K/KAy mice with genetic obesity-associated insulin resistance, a dominant negative raptor, COOH-terminally deleted raptor (raptor-ΔC_T), was overexpressed in the liver via injection of its adenovirus into the circulation. Hepatic raptor-ΔC_T expression levels were 1.5- to 4-fold that of endogenously expressed raptor. Glucose tolerance in raptor-ΔC_T-overexpressing mice improved significantly compared with that of LacZ-overexpressing mice. Insulin-induced activation of p70S6 kinase ($p70^{S6k}$) was significantly suppressed in the livers of raptor-ΔC_T overexpressing mice. In addition, insulin-induced IRS-1, Ser^{307}, and $Ser^{636/639}$ phosphorylations were significantly suppressed in the raptor-ΔC_T-overexpressing liver, whereas tyrosine phosphorylation of IRS-1 was increased. PI 3-kinase activation in response to insulin stimulation was increased approximately twofold, and Akt phosphorylation was clearly enhanced under both basal and insulin-stimulated conditions in the livers of raptor-ΔC_T mice. Thus, our data indicate that suppression of the mTOR/$p70^{S6k}$ pathway leads to improved glucose tolerance in K/KAy mice. These observations may contribute to the development of novel antidiabetic agents.

insulin receptor substrate-1; insulin resistance

THE MAMMALIAN TARGET OF RAPAMYCIN (mTOR) is a Ser/Thr kinase that belongs to the phosphatidylinositol (PI) kinase-related protein kinase family, which regulates cell growth and metabolism (7, 21). The mTOR signaling network consists of two major branches, each of which are mediated by a specific mTOR complex (mTORC) (27). The rapamycin-sensitive mTORC1 consists of mTOR, raptor, and mLST8 (also known as GβL) and regulates cell growth through effectors such as ribbosomal protein S6 kinase (S6K)1 and eukaryotic initiation factor 4E-binding protein-1 (4E-BP1) (4, 10). The rapamycin-insensitive mTORC2 contains mTOR, rictor, and mLST8 and regulates cellular proliferation through Akt (22), cytoskeleton organization through protein kinase Cα (20), and the small GTPases Rho and Rac (9).

Raptor is a large protein (150 kDa) containing a highly conserved, amino-terminal domain followed by several HEAT repeats and seven carboxy-terminal WD40 repeats (4). A number of groups (2, 12, 23) have proposed that raptor acts as an adaptor to recruit substrates p70 S6 kinase ($p70^{S6k}$) and 4E-BP1 to mTOR. Recent studies (6, 24, 26) have shown the existence of a negative feedback loop from the nutrient-sensitive TSC-mTOR-S6K1 pathway to the upstream, insulin-responsive insulin receptor substrate (IRS)-PI 3-kinase-PDK1-Akt pathway. S6K1 knockout mice were shown to be hypoinsulinemic with a decrease in β-cell mass (17). Moreover, S6K1-deficient mice are hypersensitive to insulin due to loss of the negative feedback loop from S6K1 to IRS-1 and are protected from age- and diet-induced obesity (26). Meanwhile, in genetic models of obesity, such as K/KAy and *ob/ob* mice, insulin signaling is suppressed with increased phosphorylation of Ser^{307} and $Ser^{636/639}$ in IRS-1 (26). In such mice, the activities of JNK and mTOR/S6K1, which can phosphorylate serine residue(s) of IRS-1, are reportedly elevated (8, 26).

In the present study, to elucidate the contribution of mTORC1, we overexpressed a dominant negative raptor, COOH-terminally deleted raptor (raptor-ΔC_T), using adenovirus gene transfer into the livers of K/KAy mice. Since raptor-ΔC_T binds S6K but not mTOR, raptor-ΔC_T overexpression inhibits mTOR/S6K signaling (12, 25). Under these conditions, we were able to evaluate the contribution of the mTORC1 pathway to glucose tolerance as well as signal transduction. Herein, we present data suggesting inhibition of mTORC1 to significantly enhance insulin signaling, particularly Akt activation, and thereby to ultimately improve glucose tolerance in K/KAy mice.

MATERIALS AND METHODS

Materials. Affinity-purified antibodies against IRS-1, IRS-2, phosphorylated tyrosine (4G10), S6K, and Akt/protein kinase B were prepared as previously described (11). Anti-Flag tag antibody was purchased from Sigma-Aldrich (St. Louis, MO). The antibodies against raptor, phospho-Thr^{389} of S6K, phospho-Ser^{307} and phospho-$Ser^{636/639}$ of IRS-1, phospho-$Thr^{37/46}$ and phospho-Thr^{70} of 4E-BP1, and phospho-Ser^{473} and phospho-Thr^{308} of Akt, were purchased from Cell Signaling Technology.

Address for reprint requests and other correspondence: T. Asano, Dept. of Medical Science, Graduate School of Medicine, Univ. of Hiroshima, 1-2-3 Kasumi, Minami-ku, Hiroshima City, Hiroshima, Japan 734-8553 (e-mail: asano-tky@umin.ac.jp).

The costs of publication of this article were defrayed in part by the payment of page charges. The article must therefore be hereby marked "*advertisement*" in accordance with 18 U.S.C. Section 1734 solely to indicate this fact.

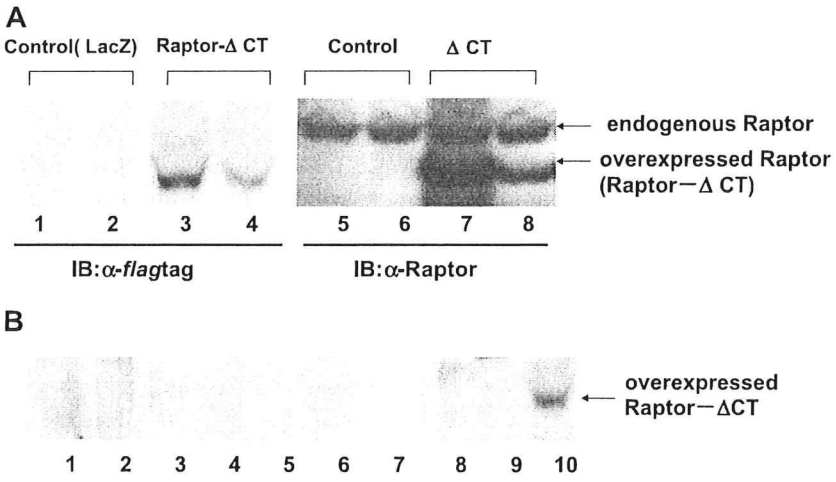

Fig. 1. The adenovirus of dominant negative raptor, COOH-terminally deleted raptor (raptor-ΔC_T). *A*: the expression levels of endogenous raptor and overexpressed raptor-ΔC_T in the livers of K/KAy mice and controls. *B*: immunoblotting (IB) of overexpressed raptor-ΔC_T in various tissues with anti-Flag tag antibody. Each tissue (30 μg), from raptor-ΔC_T-overexpressing mice, was electrophoresed and immunoblotted with anti-Flag tag antibody. *Blot 1*: brain; *blot 2*: lung; *blot 3*: heart; *blot 4*: spleen; *blot 5*: pancreas; *blot 6*: kidney; *blot 7*: fat; *blot 8*: muscle; *blot 9*: testis; *blot 10*: liver.

Adenoviruses and animals. Raptor-ΔC_T (amino acids 1–905), a dominant negative raptor, was constructed by deleting the COOH terminus of raptor. PCR was performed to amplify human raptor cDNA using a cDNA library obtained from HEK293 as a template and oligonucleotides on the basis of its reported sequence (4) as primers, yielding raptor cDNA encompassing the entire coding region. Raptor-ΔC_T (Δ, 906–1335) was generated by standard PCR-based strategies. The construct was designed to contain an Myc tag and a Flag tag at the NH_2 terminus. Recombinant adenovirus expressing β-galactosidase [i.e., the *E. coli* β -galactosidase gene (LacZ)] and COOH-terminally deleted raptor (raptor-ΔC_T) were generated, purified, and concentrated using cesium chloride ultracentrifugation, as reported previously (19). Adenovirus encoding LacZ served as a control. Male K/KAy mice, 9 wk of age, were obtained from Nippon Bio-Supp. Center (Tokyo, Japan). They were injected via the tail vein with adenovirus at a dose of 2.5×10^7 plaque-forming units/g body wt. Four days after adenovirus injection, the following experiments were performed.

Serum glucose and lipid profiles. Blood glucose was measured with a portable blood glucose monitor, Glutest-Ace R (Sanwa Kagaku Kenkyusho, Nagoya, Japan). The plasma insulin level was determined with an enzymatic immunoassay kit (Shibayagi). Serum triglyceride, cholesterol, and free fatty acids were assayed with the Triglyceride E-test, Cholesterol E-test, and NEFA C test (all from Wako Chemicals), respectively.

Intraperitoneal glucose tolerance tests. Mice were fasted for 14 h, followed by blood sampling and intraperitoneal injection of glucose (2 g/kg body wt). Whole venous blood was obtained from the tail vein at the indicated time points after the glucose load. Blood glucose was measured with a portable blood glucose monitor, as described above. We calculated the areas under the curve for glucose for each group and then compared the values obtained using Student's *t*-test.

In vivo insulin stimulation. In vivo insulin stimulation was performed as described previously (15). Mice were anesthetized with pentobarbital sodium, 0.2 ml of blood was collected from the heart, and the same amount of normal saline (0.9% NaCl), with or without insulin (1 unit/kg body wt), was then injected into the heart. The livers were removed 5 or 20 min later and immediately homogenized with a Polytron homogenizer in 10 volumes of solubilization buffer [*buffer A*: 1% Triton X-100, 20 mM Tris (pH 7.5), 150 mM NaCl, 10% glycerol, 1 mM EDTA, 100 mM sodium pyrophosphate, 100 mM sodium fluoride, 20 mM β-glycerophosphate, 2 mM sodium vanadate, 1 mM phenylmethylsulfonyl fluoride (PMSF), and 0.02 mg/ml aprotinin; *buffer B*: 137 mM NaCl, 20 mM Tris (pH 7.5), 1 mM $MgCl_2$ 1 mM $CaCl_2$, 10% glycerol, 1% NP-40, 0.05 mM sodium vanadate, 1 mM PMSF; *buffer C*: 20 mM Tris (pH 7.5), 20 mM NaCl, 1 mM EDTA, 5 mM EGTA, 1% CHAPS, 20 mM β-glycerophosphate, 1 mM sodium vanadate, 1 mM PMSF, 1 mM DTT]. The extract was centrifuged at 20,000 *g* for 15 min at 4°C, and the supernatants were used as samples for immunoprecipitation, immunoblotting (*buffer A*), or kinase assay of PI 3-kinase (*buffer B*) and S6K (*buffer C*).

Immunoprecipitation and immunoblotting. Supernatants containing equal amounts of protein (10 mg) were incubated with anti-IRS-1 and anti-S6K antibodies (3 μg/ml each) and then incubated with 45 μl of protein A- and G-Sepharose. The samples were washed and then boiled in Laemmli sample buffer containing 100 mM DTT. SDS-PAGE and immunoblotting were carried out using enhanced chemiluminescenece (ECL detection kit; Amersham), and representative blots were obtained by exposing the films. The bands were quantitatively analyzed using Molecular Imager FX (Bio-Rad) without exposure of the films.

Measurement of PI 3-kinase. For PI 3-kinase assay, the supernatants containing equal amounts of protein were immunoprecipitated for 2 h at 4°C with anti-IRS-1 or 4G10 antibody and protein A- or G-Sepharose. PI 3-kinase activities in the immunoprecipitates were assayed as described previously (14).

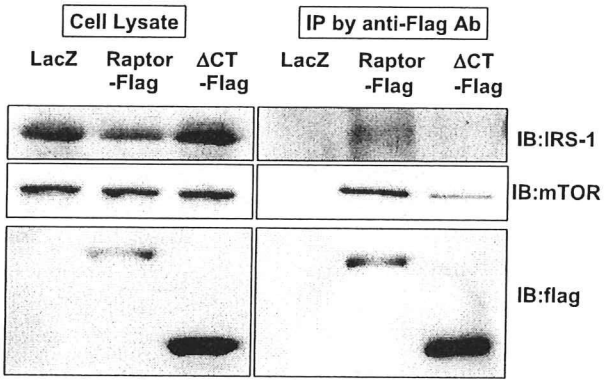

Fig. 2. COOH terminus of raptor is essential for binding with mammalian target of rapamycin (mTOR) and insulin receptor substrate-1 (IRS-1). For wild-type raptor, raptor-ΔC_T, and control (LacZ) gene transfer into HepG2 cells, the cells were incubated for 1 h in DMEM containing recombinant adenovirus. Two days later the cells were collected, and cell lysates were immunoprecipitated with Flag-tag antibody. Cell lysates and anti-Flag tag immunoprecipitates were immunoblotted with each (IRS-1, mTOR, and Flag) antibody as a probe. Representative results are shown. LacZ: $n = 3$; raptor: $n = 3$; raptor-ΔC_T: $n = 3$.

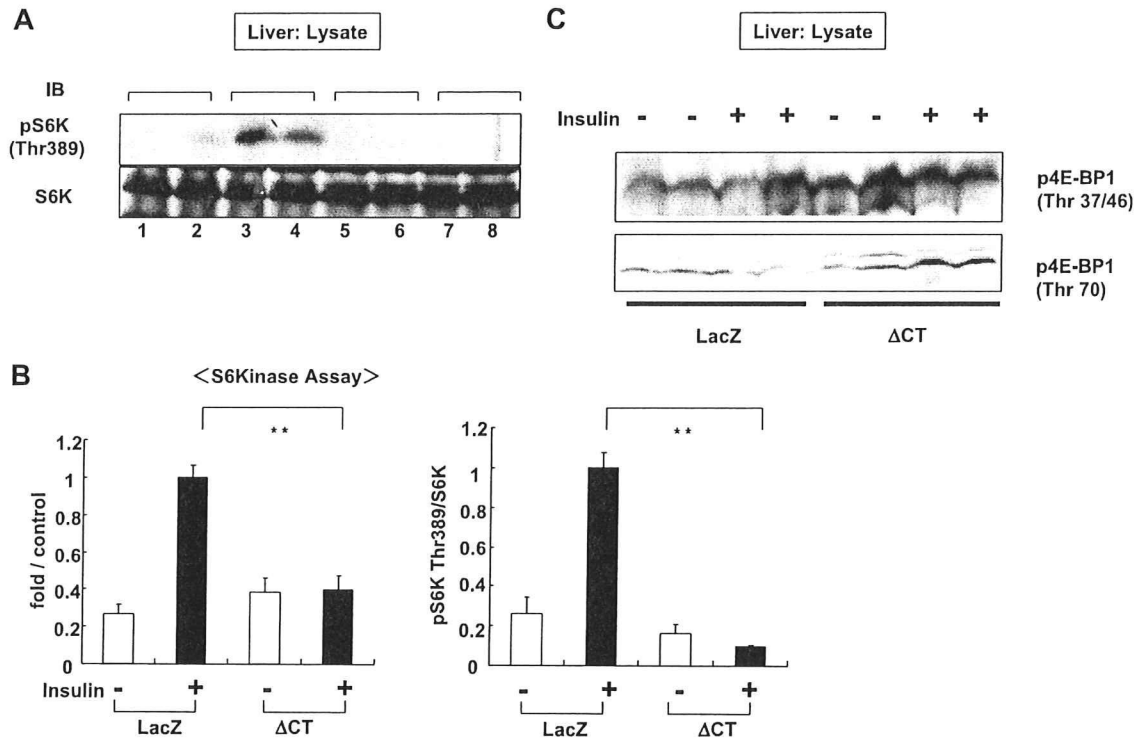

Fig. 3. Insulin-induced p70 S6 kinase ($p70^{S6k}$) activity in hepatic raptor-ΔC_T mice. The effects of raptor-ΔC_T overexpression on $p70^{S6k}$ and eukaryotic initiation factor 4E-binding protein-1 (4E-BP1) in the liver were investigated. *A*: IB of liver lysates with ribosomal S6 kinase (S6K) and phospho-S6K (Thr^{389}) antibodies revealed that insulin-induced activation of $p70^{S6k}$ was significantly depressed in the livers of raptor-ΔC_T mice. Three independent experiments were performed, and the panel shown is representative of the results. *B*: S6K assay showed insulin-induced activation of $p70^{S6k}$ to be markedly suppressed in the livers of raptor-ΔC_T overexpressing mice. LacZ: $n = 8$ ($insulin^+$: $n = 4$; $insulin^-$: $n = 4$); ΔC_T: $n = 8$ ($insulin^+$: $n = 4$; $insulin^-$: $n = 4$). $^{**}P < 0.01$. *C*: liver lysates were immunoblotted with phospho-4E-BP1 ($Thr^{37/46}$ and Thr^{70}) antibodies in 3 independent experiments, and representative results are shown. Both phosphorylations of 4E-BP1 are significantly enhanced by raptor-ΔC_T overexpression.

$p70^{S6k}$ assay. For $p70^{S6k}$ assay, the supernatants containing equal amounts of protein (10 mg) were immunoprecipitated for 2 h at 4°C with anti-S6K antibody and protein A-Sepharose. Kinase activity was analyzed using an S6K assay kit (Upstate Biotechnology, Lake Placid, NY), and the assay was carried out according to the manufacturer's instructions. In brief, the reaction mixture, containing 50 μM substrate peptide (KKRNRTLTK), inhibitor mixture [20 μM protein kinase C inhibitor peptide, 2 μM protein kinase A inhibitor peptide, and 20 μM compound R24571, an inhibitor of brain calmodulin-dependent phosphodiesterase in assay dilution buffer I (20 mM MOPS, pH 7.2, 25 mM β-glycerophosphate, 5 mM EGTA, 1 mM sodium orthovanadate, 1 mM dithiothreitol)], $p70^{S6k}$ (immunoprecipitates), and diluted [γ-^{32}P]ATP mixture were incubated for 10 min at 30°C. Then, 25 μl of the reaction mixture was spotted onto p81 phosphocellulose squares. Intensities of the resultant bands were determined using BAS2000 (Fuji Film).

Statistical analysis. Results are expressed as means ± SE. Comparisons were made using one-way ANOVA followed by the Tukey test and the unpaired Student *t*-test. Values of $P < 0.05$ were considered statistically significant.

RESULTS

Overexpression of raptor-ΔC_T markedly suppressed insulin-induced activation of $p70^{S6k}$ in the livers of K/KAy mice. To examine levels of endogenously expressed raptor and raptor-ΔC_T in the liver, we carried out immunoblotting with anti-Flag tag or anti-raptor antibody. Raptor-ΔC_T expressions were identified by immunoblotting with anti-Flag tag antibody in raptor-ΔC_T-overexpressing mice, but not in controls (Fig. 1). Immunoblotting with the anti-raptor antibody detected both endogenous raptor and overexpressed raptor-ΔC_T, and the levels of

Table 1. *Weights and metabolic profiles of LacZ and raptor-ΔC_T-overexpressing mice*

	LacZ	Raptor-ΔC_T
BW, g (*day 1*)	36.3±1.04	36.6±1.2
BW, g (*day 5*)	36.9±1.1	37±1.27
Liver/BW × 10^2 (*day 5*)	4.87±0.44	5.12±0.34
Fat/BW × 10^2 (*day 5*)	4±0.62	3.9±0.32
Heart/BW × 10^2 (*day 5*)	0.37±0.25	0.48±0.01
Kidney/BW × 10^2 (*day 5*)	0.94±0.62	1.28±0.02
FBS, mg/dl (*day 1*)	122±7.48	126±9.03
FBS, mg/dl (*day 5*)	160±6.31	140±8.37
T-cho, mg/dl (*day 5*)	123±10.8	125±7.96
TG, mg/dl (*day 5*)	197±83.2	200±48.2
NEFA, mEq/l (*day 5*)	0.79±0.13	0.88±0.22
Insulin, ng/ml (*day 5*)	2.36±1.78	0.91±0.34

Values are means ± SE. LacZ, control; raptor-ΔC_T, COOH-terminally deleted raptor; BW, body weight; FBS, fasting blood sugar; T-cho, total cholesterol; TG, triglyceride; NEFA, nonesterified fatty acid. The body weights, major organ weights, blood glucose levels, and lipid concentrations of LacZ and Raptor-ΔCT mice, before and 4 days after adenovirus injection, are shown. LacZ: $n = 8$; raptor-ΔC_T: $n = 8$.

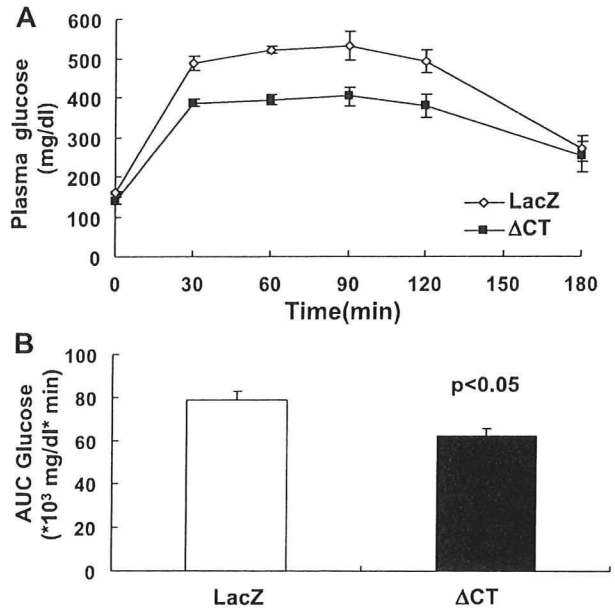

Fig. 4. Significantly lower glucose levels in raptor-ΔC_T mice after glucose tolerance test (GTT). Mice were fasted for 14 h, followed by blood sampling and intraperitoneal injection of glucose (2 g/kg body wt). *A*: whole venous blood was obtained from the tail vein at the indicated time points after the glucose load. *B*: areas under the curve (AUC) for glucose for each group were calculated and compared using the Student *t*-test. Intraperitoneal GTT revealed hepatic raptor-ΔC_T overexpression to improve glucose tolerance. LacZ: $n = 4$; raptor-ΔC_T: $n = 4$. $^*P < 0.05$.

raptor-ΔC_T were ~1.5- to fourfold that of endogenously expressed raptor (Fig. 1*A*). In addition, overexpression of raptor-ΔC_T was limited to the liver; i.e., none was detected by immunoblotting of other tissues (Fig. 1*B*). (Faint bands in the lung, heart, and kidney were nonspecific.) Next, we investigated the associations of wild-type raptor and raptor-ΔC_T with mTOR or IRS-1. As shown in Fig. 2, IRS-1 and mTOR were detected in the Flag-tagged raptor immunoprecipitates. In contrast, it was revealed that raptor-ΔC_T had lost the ability to associate with IRS-1, and the association of raptor-ΔC_T with mTOR was also much weaker than that of wild-type raptor. Thus, it was suggested that raptor-ΔC_T functions as a dominant negative construct.

Subsequently, the effect of raptor-ΔC_T overexpression on $p70^{S6k}$ activity was investigated in the liver. S6K assay and immunoblotting of liver lysates with S6K and phospho-S6K (Thr^{389}) antibodies revealed insulin-induced activation of $p70^{S6k}$ to be markedly suppressed in the livers of raptor-ΔC_T-overexpressing mice (Fig. 3, *A* and *B*). However, surprisingly, 4E-BP1 phosphorylations of both Thr^{37} and Thr^{46} were significantly increased by raptor-ΔC_T overexpression under both basal and insulin-stimulated conditions, and that of Thr^{70} was also increased in the insulin-stimulated state (Fig. 3*C*).

Weights and metabolic profiles of control (LacZ) and raptor-ΔC_T-overexpressing mice. The body weights, major organ weights, blood glucose levels, and lipid concentrations of raptor-ΔC_T mice did not differ from those of control mice either before or 4 days after adenovirus injection. Fasting serum insulin levels of raptor-ΔC_T mice were lower, but not significantly (Table 1).

Hepatic raptor-ΔC_T overexpressing mice showed a profound increase in glucose tolerance. To investigate the effect of hepatic raptor-ΔC_T overexpression on glucose tolerance, we performed intraperitoneal glucose tolerance tests (Fig. 4*A*). Blood glucose levels of raptor-ΔC_T mice were significantly lower than those of control mice (Fig. 4*B*).

Hepatic raptor-ΔC_T overexpression enhanced insulin signaling associated with decreased IRS-1 Ser^{307} and $Ser^{636/639}$ phosphorylation in K/KAy mice. As shown in Fig. 5*A*, there were no

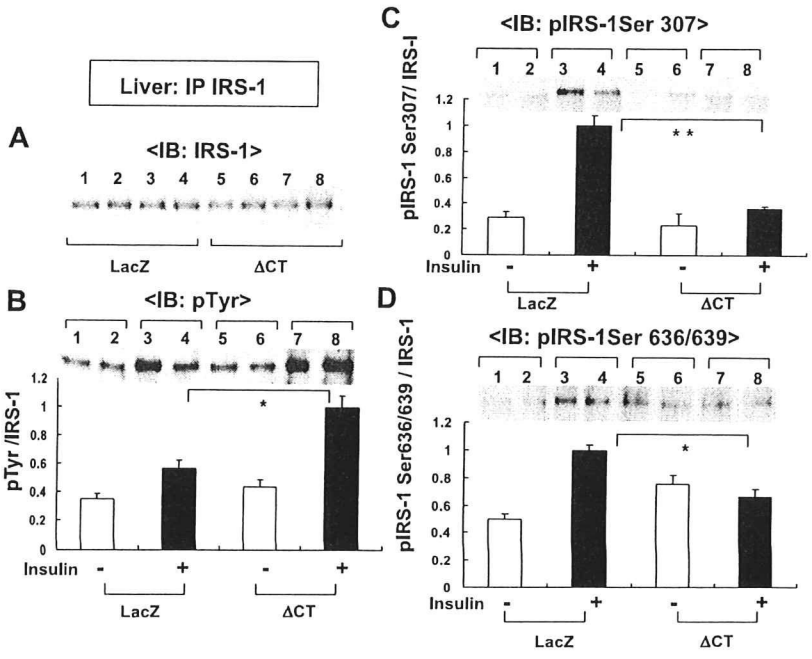

Fig. 5. Insulin-induced IRS-1 tyrosine residue and Ser^{307} and $Ser^{636/639}$ phosphorylations in hepatic raptor-ΔC_T mice. Four days after adenovirus injection the livers were removed after insulin or saline administration, followed by immunoprecipitation (IP) with IRS-1 antibody. SDS-PAGE and IB were then performed using the appropriate antibody as a probe. *A*: there was no difference between raptor-ΔC_T and control mice in the expression of IRS-1 protein. *B*: insulin-induced IRS-1 tyrosine phosphorylation was significantly increased in raptor-ΔC_T mice. *C* and *D*: insulin-induced IRS-1 Ser^{307} and $Ser^{636/639}$ phosphorylations were markedly depressed in raptor-ΔC_T mice. LacZ: $n = 8$ (insulin$^+$: $n = 4$; insulin$^-$: $n = 4$); ΔC_T: $n = 8$ (insulin$^+$: $n = 4$; insulin$^-$: $n = 4$). $^*P < 0.05$; $^{**}P < 0.01$.